remote sensing

MDPI

Article

Geotechnologies in Biophysical Analysis through the Applicability of the UAV and Sentinel-2A/MSI in Irrigated Area of Common Beans: Accuracy and Spatial Dynamics

Henrique Fonseca Elias de Oliveira [1,2,*], Lucas Eduardo Vieira de Castro [1], Cleiton Mateus Sousa [1,2], Leomar Rufino Alves Júnior [3], Marcio Mesquita [2,4], Josef Augusto Oberdan Souza Silva [2], Lessandro Coll Faria [5], Marcos Vinícius da Silva [6], Pedro Rogerio Giongo [7], José Francisco de Oliveira Júnior [8], Vilson Soares de Siqueira [9] and Jhon Lennon Bezerra da Silva [2]

[1] Faculty of Agronomy, Goiano Federal Institute—Campus Ceres, GO-154, km 218—Zona Rural, Ceres 76300-000, Goiás, Brazil; lucas.castro@estudante.ifgoiano.edu.br (L.E.V.d.C.); cleiton.sousa@ifgoiano.edu.br (C.M.S.)
[2] Cerrado Irrigation Graduate Program, Goiano Federal Institute—Campus Ceres, GO-154, km 218—Zona Rural, Ceres 76300-000, Goiás, Brazil; marcio.mesquita@ufg.br (M.M.); josef.silva@estudante.ifgoiano.edu.br (J.A.O.S.S.); jhon.silva@ifgoiano.edu.br (J.L.B.d.S.)
[3] Laboratory for Image Processing and Geoprocessing, Federal University of Goiás, Goiânia 74690-900, Goiás, Brazil; leomar.junior@ifg.edu.br
[4] Faculty of Agronomy, Federal University of Goiás (UFG), Nova Veneza, km 0. Campus Samambaia—UFG, Goiânia 74690-900, Goiás, Brazil
[5] Center of Technological Development, Federal University of Pelotas, Pelotas 96010-610, Rio Grande do Sul, Brazil; lessandro.faria@ufpel.edu.br
[6] Department of Agricultural Engineering, Federal Rural University of Pernambuco, Rua Dom Manoel de Medeiros, Dois Irmãos, Recife 52171-900, Pernambuco, Brazil; marcolino_114@hotmail.com
[7] Department of Agricultural Engineering, State University of Goiás, Via Protestato Joaquim Bueno, 945, Perímetro Urbano, Santa Helena de Goiás 75920-000, Goiás, Brazil; pedro.giongo@ueg.br
[8] Institute of Atmospheric Sciences (ICAT), Federal University of Alagoas (UFAL), Maceió 57072-260, Alagoas, Brazil; jose.junior@icat.ufal.br
[9] Faculty of Information Systems, Goiano Federal Institute—Campus Ceres, GO-154, km 218—Zona Rural, Ceres 76300-000, Goiás, Brazil; vilson.soares@ifgoiano.edu.br
* Correspondence: henrique.fonseca@ifgoiano.edu.br

Abstract: The applicability of remote sensing enables the prediction of nutritional value, phytosanitary conditions, and productivity of crops in a non-destructive manner, with greater efficiency than conventional techniques. By identifying problems early and providing specific management recommendations in bean cultivation, farmers can reduce crop losses, provide more accurate and adequate diagnoses, and increase the efficiency of agricultural resources. The aim was to analyze the efficiency of vegetation indices using remote sensing techniques from UAV multispectral images and Sentinel-2A/MSI to evaluate the spectral response of common bean (*Phaseolus vulgaris* L.) cultivation in different phenological stages (V4 = 32 DAS; R5 = 47 DAS; R6 = 60 DAS; R8 = 74 DAS; and R9 = 89 DAS, in 99 days after sowing—DAS) with the application of doses of magnesium (0, 250, 500, and 1000 g ha^{-1}). The field characteristics analyzed were mainly chlorophyll content, productivity, and plant height in an experimental area by central pivot in the midwest region of Brazil. Data from UAV vegetation indices served as variables for the treatments implemented in the field and were statistically correlated with the crop's biophysical parameters. The spectral response of the bean crop was also detected through spectral indices (NDVI, NDMI_GAO, and NDWI_GAO) from Sentinel-2A/MSI, with spectral resolutions of 10 and 20 m. The quantitative values of NDVI from UAV and Sentinel-2A/MSI were evaluated by multivariate statistical analysis, such as principal components (PC), and cophenetic correlation coefficient (CCC), in the different phenological stages. The NDVI and MCARI vegetation indices stood out for productivity prediction, with r = 0.82 and RMSE of 330 and 329 kg ha^{-1}, respectively. The TGI had the best performance in terms of plant height (r = 0.73 and RMSE = 7.4 cm). The best index for detecting the relative chlorophyll SPAD content was MCARI (r = 0.81; R^2 = 0.66 and RMSE = 10.14 SPAD), followed by NDVI (r = 0.81;

check for updates

Citation: de Oliveira, H.F.E.; de Castro, L.E.V.; Sousa, C.M.; Alves Júnior, L.R.; Mesquita, M.; Silva, J.A.O.S.; Faria, L.C.; da Silva, M.V.; Giongo, P.R.; de Oliveira Júnior, J.F.; et al. Geotechnologies in Biophysical Analysis through the Applicability of the UAV and Sentinel-2A/MSI in Irrigated Area of Common Beans: Accuracy and Spatial Dynamics. *Remote Sens.* **2024**, *16*, 1254. https://doi.org/10.3390/rs16071254

Academic Editors: Prasad S. Thenkabail and Jochem Verrelst

Received: 18 January 2024
Revised: 15 March 2024
Accepted: 28 March 2024
Published: 1 April 2024

Copyright: © 2024 by the authors. Licensee MDPI, Basel, Switzerland. This article is an open access article distributed under the terms and conditions of the Creative Commons Attribution (CC BY) license (https://creativecommons.org/licenses/by/4.0/).

R^2 = 0.65 and RMSE = 10.19 SPAD). The phenological stage with the highest accuracy in estimating productive variables was R9 (Physiological maturation). GNDVI in stages R6 and R9 and VARI in stage R9 were significant at 5% for magnesium doses, with quadratic regression adjustments and a maximum point at 500 g ha^{-1}. Vegetation indices based on multispectral bands of Sentinel-2A/MSI exhibited a spectral dynamic capable of aiding in the management of bean crops throughout their cycle. PCA (PC1 = 48.83% and PC2 = 39.25%) of the satellite multiple regression model from UAV vs. Sentinel-2A/MSI presented a good coefficient of determination (R^2 = 0.667) and low RMSE = 0.12. UAV data for the NDVI showed that the Sentinel-2A/MSI samples were more homogeneous, while the UAV samples detected a more heterogeneous quantitative pattern, depending on the development of the crop and the application of doses of magnesium. Results shown denote the potential of using geotechnologies, especially the spectral response of vegetation indices in monitoring common bean crops. Although UAV and Sentinel-2A/MSI technologies are effective in evaluating standards of the common bean crop cycle, more studies are needed to better understand the relationship between field variables and spectral responses.

Keywords: remote sensing; multispectral images; NDVI; multiple regression; *Phaseolus vulgaris* L.

1. Introduction

Remote sensing, through electromagnetic radiation–plant–sensor interaction, has a high potential for identifying crop conditions because it allows non-destructive assessment quickly and at a relatively low cost [1–3]. This tool can be used to define areas for specific management, manage crop fertilization and irrigation [4], control weeds, and estimate crop productivity [5,6], presenting high practical importance, helping producers manage their production and define the price of agricultural products [7].

The increase in mapping and geospatial diagnosis levels through remote sensing techniques varies widely and provides effective support for constant applications in worldwide crop growth research [8,9]. The combination of agronomic data with orbital sensors and UAV data enhances the level of information and improves the reliability of geospatial and field data, aiming to optimize crop management [3]. However, it is necessary to align the spectral and temporal resolution of orbital sensors, as satellites with coarse resolution may not efficiently detect agricultural fields. The Sentinel-2A/MSI satellite of the Copernicus Program by the European Space Agency (ESA) is one of the satellites providing free geospatial data availability, offering multispectral images with a high spectral resolution pixel of 10 m, and a temporal resolution of just 5 days, characteristics that provide a significant advantage for monitoring agricultural cycles.

Unmanned Aerial Vehicles (UAVs) have gained increasing traction in the agricultural sector [10–13]. Such a tool can be defined as a set of elements composed of a UAV, its respective remote piloting station, the piloting link, and other components necessary for operation [14]. When integrated with optical sensors, the UAV can be a reliable tool for rapid phenotyping under field conditions [15]. Onboard sensors can capture data at high throughput and generate multiple graphs at the desired spatiotemporal resolution [16]. This indicates that the next agricultural revolution will be driven by the intelligent use of data that could increase productivity and contribute to environmental sustainability through the rational use of resources [17].

The use of geotechnologies is an example of significant advances for irrigated agriculture in the midwest region of Brazil, specifically the sets of remote sensing techniques extracted by the applicability of UAVs and satellites/sensors, which are efficient in detecting multispectral responses. In other words, they promote results due to the digital processing of multispectral images with machine learning technologies and highly specific mathematical modeling using software and geographic information systems (GIS), to assist in the behavior pattern and spatiotemporal diagnosis of crops. Given the significant challenges in assessing the spatial variability of agricultural practices through field surveys,

which are highly costly and time-consuming tasks [18,19], the region lacks studies with this innovation in the field of agricultural remote sensing, which involves integrating field data and data from orbital and UAV sensors, at different spatial and temporal scales. This approach allows for a more precise analysis of crop conditions, optimizing agricultural management and providing valuable insights to increase the productivity and environmental sustainability of the region. Considering that agriculture also faces significant pressures on soil coverage and water resources, and in times of climate change, these pressures are intensified.

Several vegetation indices can be utilized for remote sensing of agricultural areas, according to various pieces of research [15,20–22], which are mathematical models constructed from the reflectance of the vegetative canopy, provided in different spectral bands and wavelengths of the electromagnetic spectrum, mainly in the visible (RGB) and near-infrared (NIR) bands [23,24]. These wavelengths provide crucial information about vegetation [25]. These indices are designed to emphasize vegetation vigor and properties such as chlorophyll content, radiation, uptake, and reflection by canopy biomass [20,26,27]. Measuring leaf reflectance or transmittance of photosynthetic pigments is a promising method for monitoring crop growth, planning nutritional management, and estimating yield [28].

Given the variety of existing vegetation indices, studies are needed to determine the best indices and phenological stages of evaluation that present the greatest accuracy in estimating the agronomic attributes of each crop, ensuring the application of remote sensing with greater precision [5,12,16]. Correlations between grain yield and vegetation indices obtained from a single data point must be viewed with caution, as cumulative data of the indices during the crop cycle can better estimate yield [29]. Several authors have reported better performance of prediction models based on multitemporal remote sensing data, compared to models based on single-stage data, in different crops [30–34]. In this scenario, among the crops with high economic potential and social impact, capable of justifying investment in new technologies and monitoring methods, the common bean (*Phaseolus vulgaris* L.) stands out [15,18,35]. However, productivity remains low due to the crop's high demand for soil fertility, owing to its short cycle and superficial and poorly developed root systems, which necessitate nutrient availability according to demand during the cycle. Therefore, macronutrients such as magnesium (Mg) must be readily available to plants according to demand during the cycle [36]. In adequate amounts, Mg can contribute to the improvement of the nutritional status and grain productivity, directly associated with the quality of agricultural products and the maintenance of high productivity rates [37,38].

Unlike other research that studied UAV remote sensing individually, in some cases only with RGB images [39–41], this research provides a technological diagnosis of responses to the evaluations and measurements of beans in situ, up to patterns of the responses observed by multispectral UAV images and orbital satellite images. The joint analysis of the UAV with orbital sensors allows us to expand the horizons of the multiple tools to be applied in monitoring crops such as common beans. This monitoring allows the determination of specific biophysical indices (e.g., Normalized Difference Vegetation Index—NDVI; Green Normalized Difference Vegetation—GNDVI), which reinforce the diagnosis of vegetation health during the crop cycle from different sensors.

In the current context of geotechnologies, exploring the orbital sensors/models requires a necessary analysis to minimize technological costs and improve the results obtained. Providing viable alternatives in agricultural monitoring brings a range of options for small, medium, and large rural producers, mainly to overcome specific challenges such as disease and pest management, and environmental stresses. By identifying these problems early and providing specific management recommendations, farmers can reduce crop losses and increase the efficiency of agricultural resources. This approach has the potential to radically transform how we grow food and manage our natural resources, benefiting farmers, consumers, and the environment. In this context, the aim was to analyze the feasibility and efficiency of vegetation indices derived from multispectral and RGB images, using sets of remote sensing techniques from UAV image data and the Sentinel-2A/MSI satellite, to

evaluate and monitor the spectral dynamics and performance of common bean (*Phaseolus vulgaris* L.) cultivation as a function of foliar application of doses of magnesium in the different phenological stages of the crop in an experimental area by central pivot in the midwest region of Brazil.

2. Materials and Methods

2.1. Experimental Site

The study was conducted in the experimental area of the Goiano Federal Institute—*Campus* Ceres, located in Ceres, state of Goiás, in the midwest region of Brazil. The coordinates of the experimental site are 15°21′16″S latitude and 49°36′23″W longitude, with an altitude of 570 m. The cultivation area was under a central pivot system, with specific coordinates of 15°21′17.2″S latitude and 49°36′23.2″W longitude, and an altitude of 560 m (Figure 1). The study focused on the cultivation of the common bean, specifically the BRS style variety, which exhibits an indeterminate growth habit and has an average growth cycle of 90 to 100 days. The soil in the area is classified as Oxisol. The study period spanned from 17 June 2021 to 24 September 2021 [42,43].

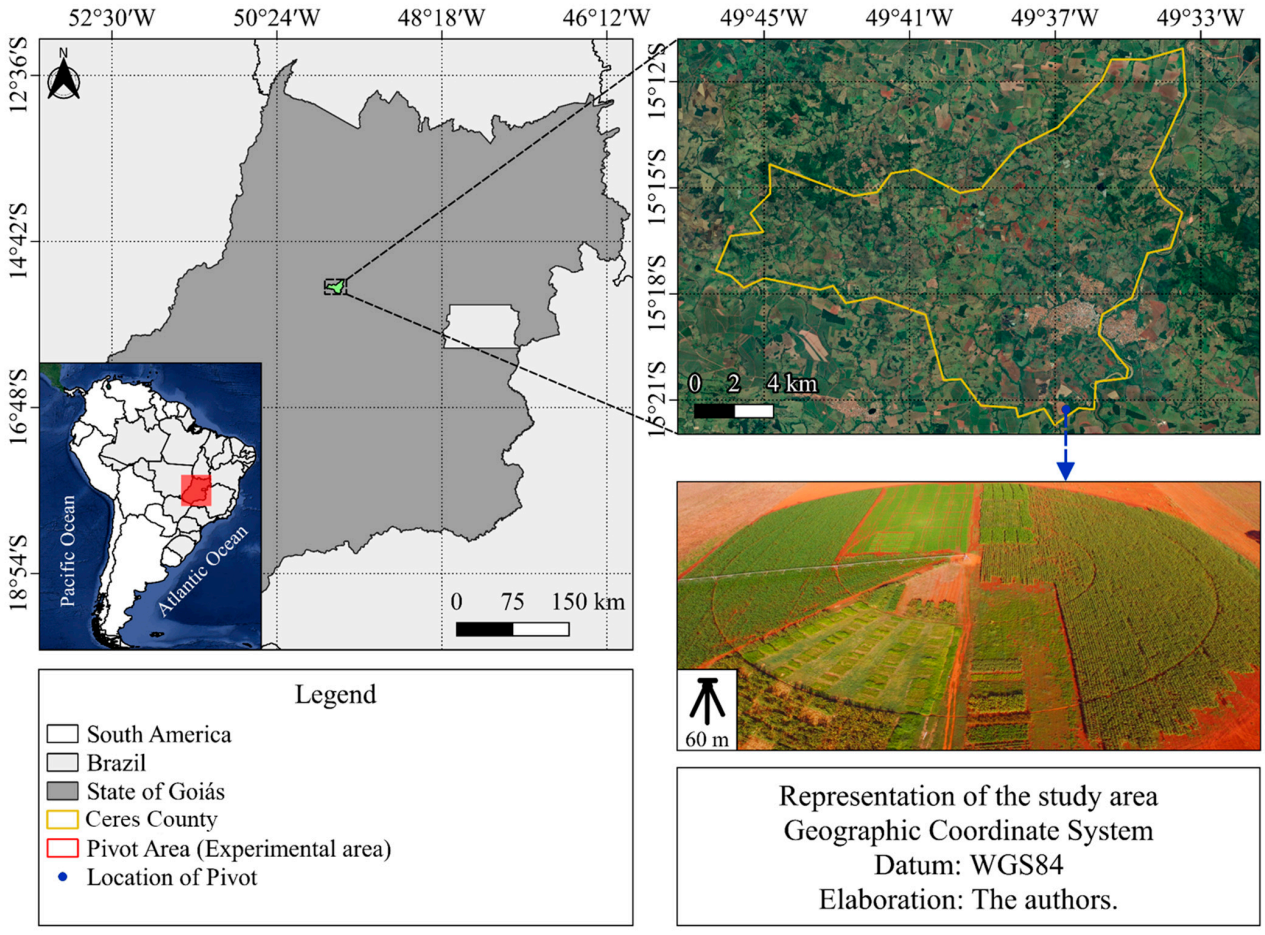


Figure 1. Spatial location of the experimental study area under a pivot for recording the UAV images (spatial resolution of 60 m) in Ceres County, Goiás, Brazil.

According to the Köppen classification [44], the local climate is type Aw (Tropical humid and dry), with dry winters and rainy summers, an average annual temperature of 25 °C, and average annual precipitation above 1300 mm. Climatic data were recorded using a weather station (Vantage Pro 2; Davis; Hayward, CA, USA). There was no precipitation during the experiment and the water needs of the crops were met via irrigation. The

mean temperature, evapotranspiration, and relative humidity were 22.86 °C, 4.19 mm, and 59.43%, respectively (Figures 2 and 3).

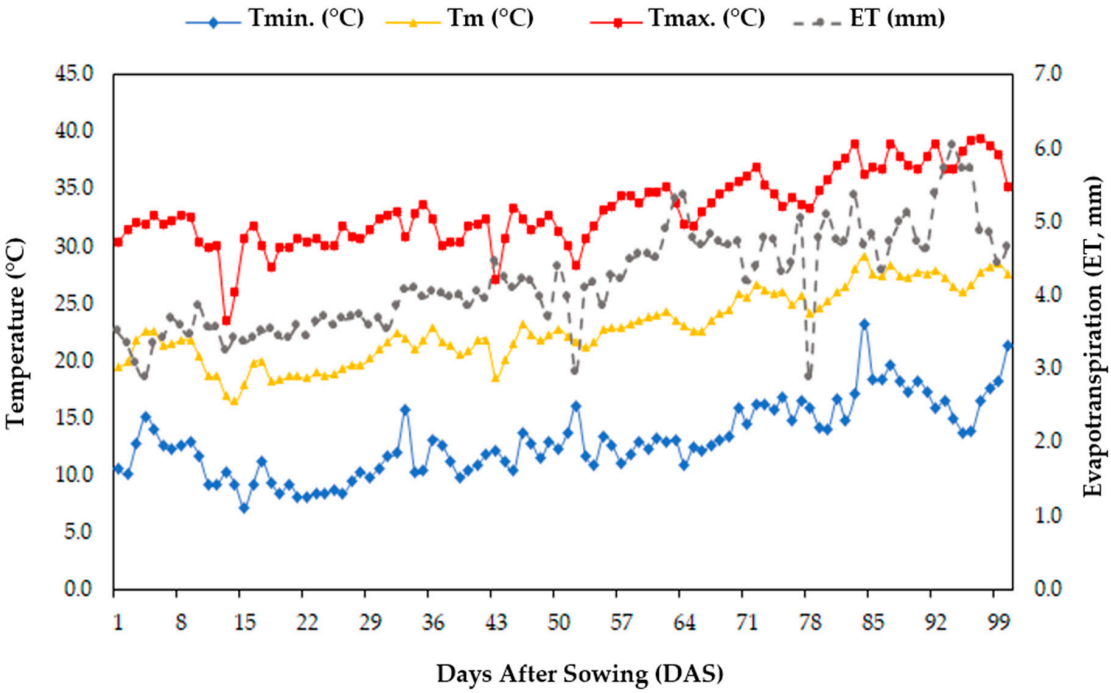


Figure 2. Meteorological data of minimum (Tmin.), mean (Tm), and maximum (Tmax.) temperature and evapotranspiration (ET, mm) as a function of Days After Sowing (DAS).

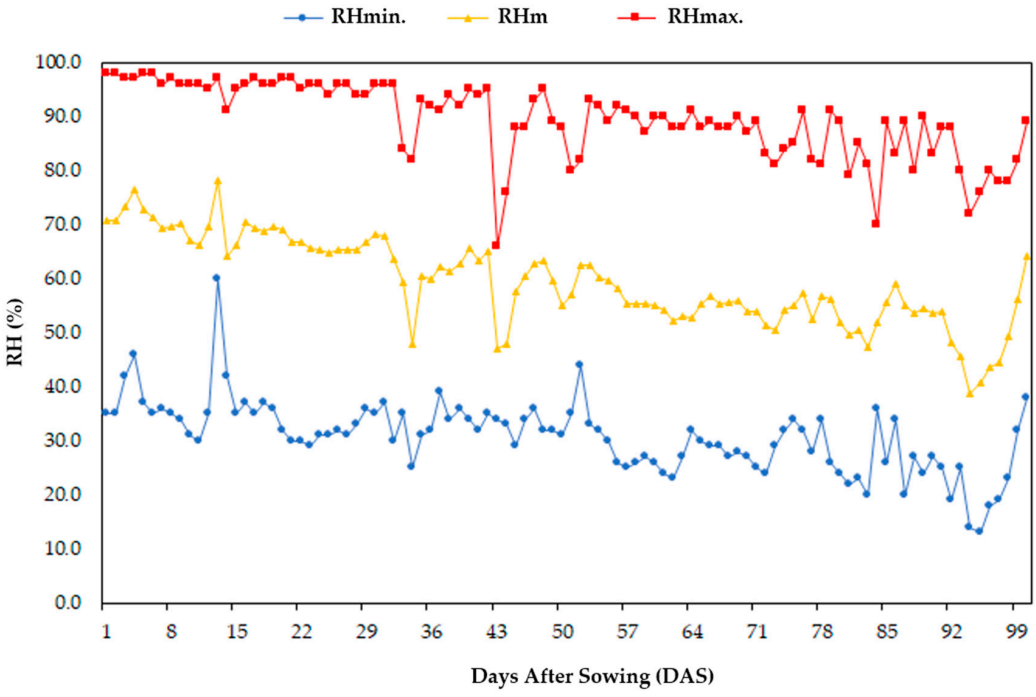


Figure 3. Data of minimum (RHmin.), mean (RHm), and maximum (RHmax.) relative air humidity (RH, %) as a function of days after sowing (DAS).

The experimental design used was randomized blocks, in a 4 × 2 factorial scheme, with 4 doses of magnesium (magnesium sulfate—$MgSO_4$): 0, 250, 500, and 1000 g ha^{-1}, applied via the leaves at 27 and 56 days after sowing (DAS), corresponding to two phenological stages of the crop (V4—third developed trefoil and R6—full bloom). The contour

experiment had 4 replications (blocks), each with 8 plots corresponding to the respective treatments, totaling 32 plots. The plots were composed of 8 rows of 5.0 m in length, spaced at 0.5 m, totaling 20 m^2, containing 12 seeds per linear meter (240,000 plants ha^{-1}). The estimates were made on the central lines, disregarding 0.5 m at the ends.

2.2. Field Characteristics Analyzed

The chlorophyll content was determined using a portable meter (Minolta, Mod. SPAD 502), analyzing three plants per plot, selecting leaves with more intense green colors, and fully expanded and without lesions. The readings were taken at 32, 47, 60, 74, and 89 DAS, corresponding to the phenological stages V4 (complete opening of the third trefoil), R5 (presence of the first flower buds), R6 (full flowering), R8 (filling of grains) and the beginning of the R9 stage (leaf senescence and regulatory control of grains), respectively, thus seeking to contemplate the entire crop cycle after the first magnesium application.

At the time of harvest at 99 DAS, productivity (kg ha^{-1}), and plant height (cm) were determined by measuring the length of the main branch, mass of 1000 grains (g), number of branches per plant, pods per plant, and number of grains per pod.

2.3. Image Acquisition and Digital Processing Analytics (from UAV)

Figure 4 shows a flowchart of the image acquisition process until the data of interest were obtained.

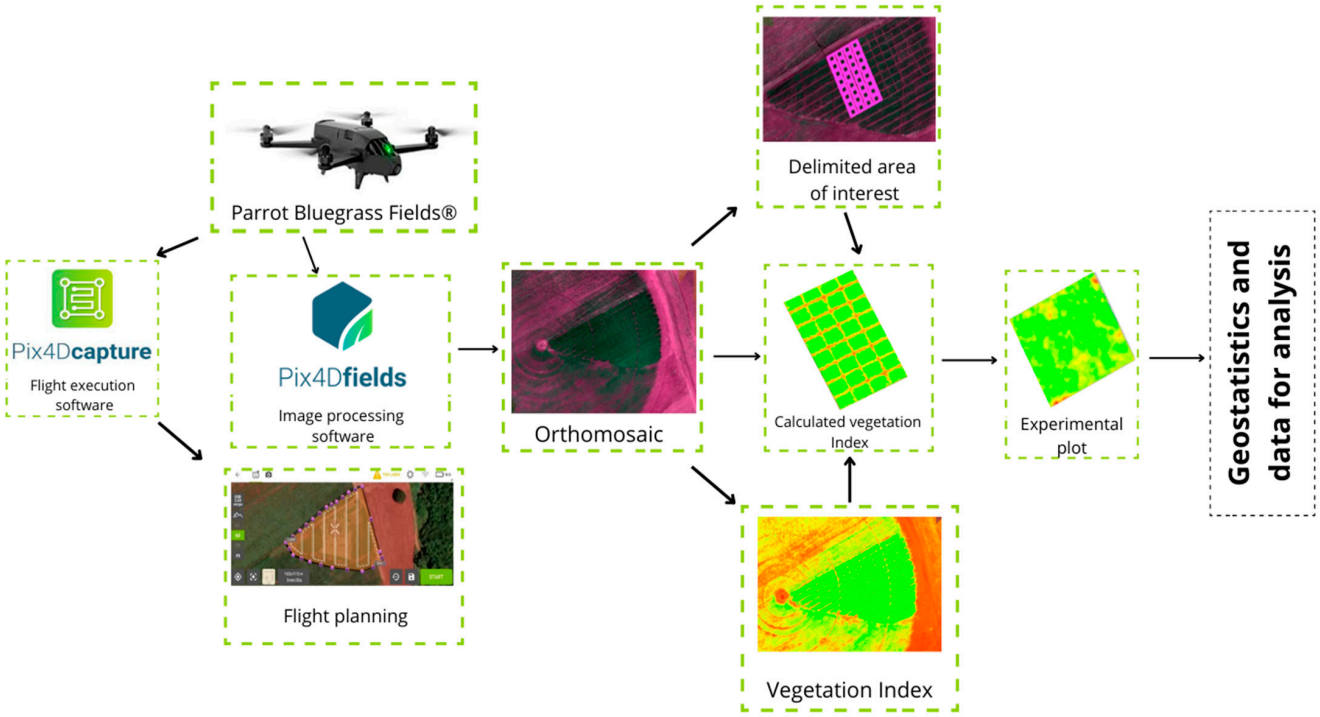


Figure 4. Flowchart of image acquisition and processing and data collection of vegetation indices.

The images were obtained by remotely piloted aircraft (RPA), via Parrot Bluegrass Fields® multirotor drone (Parrot Drones S.A, Paris, France), equipped with a Parrot Sequoia® sensor from the same manufacturer, which collected RGB images, in the visible spectrum (Red, Green, and Blue (450 to 690 nm)) and multispectral in 4 different bands: Green (550 nm +/− 40 nm), Red (660 nm +/− 40 nm), RedEdge (735 nm +/− 10 nm) and NIR (790 nm +/− 40 nm). This type of sensor performs radiometric self-calibration of images in real time, using a solar sensor integrated into a camera.

The flights were performed at a standard altitude of 60 m, always between 11:00 am and 01:00 pm to avoid the presence of shadows, with a frontal and lateral overlap of 80%, generated in spatial resolution between 6.0 and 6.19 cm/pixel for multispectral images and

4.0 and 4.25 cm/pixel for RGB images. All flights were planned and executed using Pix4D Capture® software (Pix4D SA, Lausanne, Switzerland), and the images were processed using Pix4D Fields® software (Pix4D SA, Lausanne, Switzerland), where orthomosaics and geostatistical data were generated. For each phenological stage of interest (V4, R5, R6, R8, and R9, corresponding to 32, 47, 60, 74, and 89 DAS), two orthomosaics were generated, one from the UAV multispectral images (Figure 5), and the other from the RGB images.

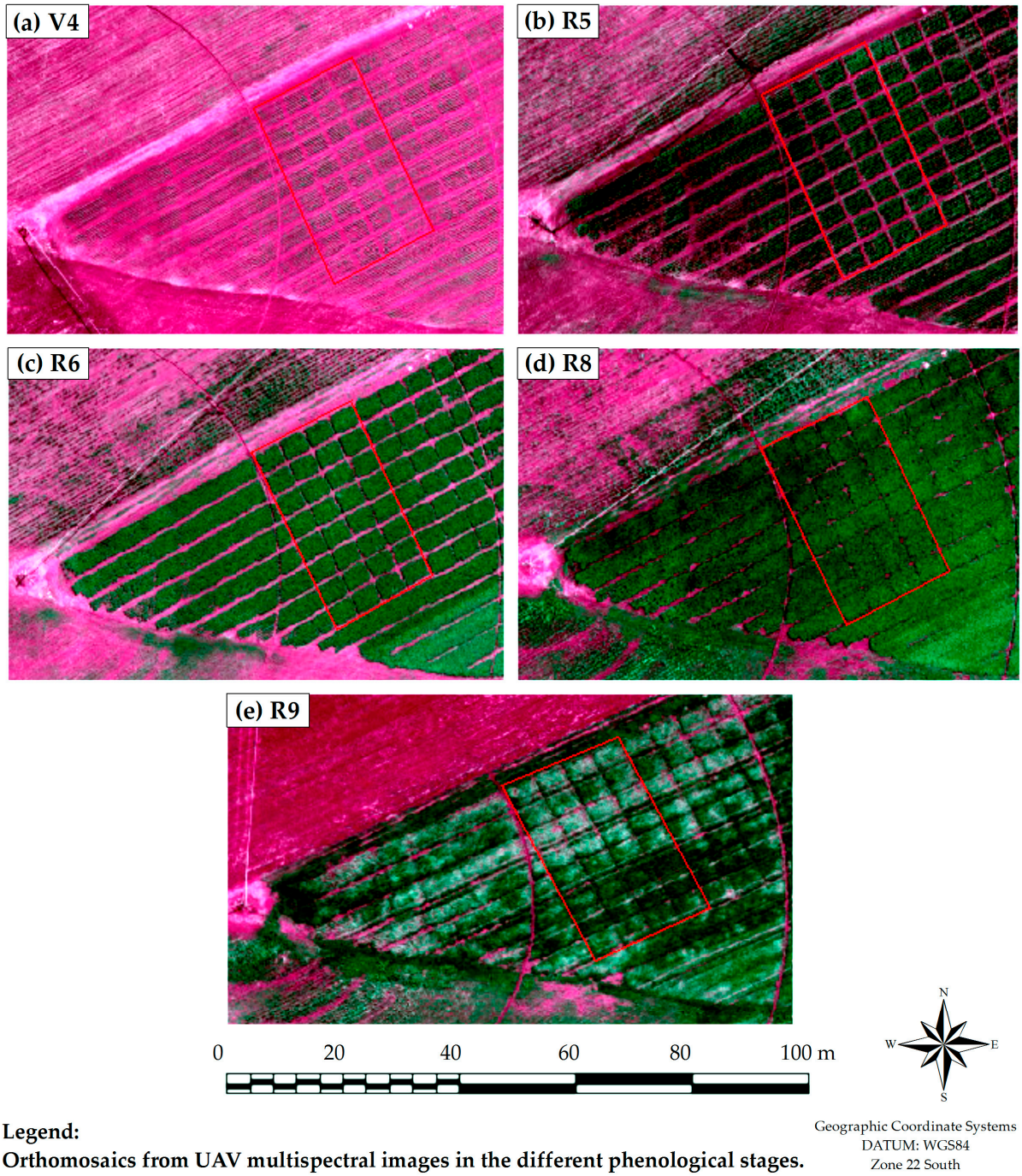


Figure 5. Orthomosaics in false color, generated from UAV multispectral images. (**a**) V4: complete opening of the third trefoil; (**b**) R5: presence of the first flower buds; (**c**) R6: full flowering; (**d**) R8: grain filling; (**e**) R9: leaf senescence and grain regulation. The experimental area is demarcated by the red polygon.

2.4. Biophysical Indices (from UAV)

Areas of 16 m^2 were delimited in each orthomosaic in each plot, thus discarding 4 m^2 borders. Subsequently, the vegetation indices were calculated and extracted (Table 1), using the average of each index per plot in the analysis. Via UAV, the main indices are, for multispectral images, as follows: Normalized Difference Vegetation Index (NDVI), Green Normalized Difference Vegetation Index (GNDVI), Normalized Difference Red Edge Index (NDRE), Modified Chlorophyll Absorption in Reflective Index (MCARI), Leaf Chlorophyll Index (LCI), and Structure Insensitive Pigment Index 2 (SIPI2); RGB images: Visible Atmospherically Resistant Index (VARI) and Triangular Greenness Index (TGI). The data from the vegetation indices served as a variable for the treatments in the field and were statistically correlated with the biophysical parameters of the crop.

Table 1. Vegetation indices, equations using spectral bands, and references.

Vegetation Indices	Acronym	Equation	References
Normalized Difference Vegetation Index	NDVI	$\frac{pNIR-pRed}{pNIR+pRed}$	[45]
Green Normalized Difference Vegetation Index	GNDVI	$\frac{pNIR-pGreen}{pNIR+pGreen}$	[46]
Normalized Difference Red Edge Index	NDRE	$\frac{pNIR-pRedEdge}{pNIR+pRedEdge}$	[47]
Modified Chlorophyll Absorption in Reflective Index	MCARI	$\frac{[(p700-p670)-0.2(p700-p550)]p700}{p670}$	[48]
Leaf Chlorophyll Index	LCI	$\frac{pNIR-pRedEdge}{pNIR+pRed}$	[49]
Structure Insensitive Pigment Index 2	SIPI2	$\frac{pNIR-pGreen}{pNIR-pRed}$	[50]
Visible Atmospherically Resistant Index	VARI	$\frac{pGreen-pRed}{pGreen+pRed-pBlue}$	[51]
Triangular Greenness Index	TGI	$pGreen - 0.39pRed - 0.61pBlue$	[52]

where p indicates the reflectance in each of the bands in nanometers (nm).

2.5. Orbital Data of Satellite (from Sentinel-2A/MSI)

The study was also followed over time by images from the Sentinel-2A/MSI satellite from the Multispectral Instrument (MSI) sensor, Level-2A processing (Table 2), where geospatial analysis was developed based on indicator indices sensitive to soil spectral change conditions. Highlighting the Normalized Difference Vegetation Index (NDVI) [53–56], Normalized Difference Moisture Index (NDMI_GAO), and the Normalized Difference Water Index (NDWI_GAO) [57,58].

Table 2. Characteristics of the multispectral bands used in the study, Sentinel-2A/MSI.

Band Name	Center Wavelength	Temporal Resolution	Spatial Resolution	Radiometric Resolution	Processing Level
r_{GREEN}	560 nm	10/5 days	10 m	16 bits	L2A
r_{RED}	665 nm	10/5 days	10 m	16 bits	L2A
r_{NIR}	842 nm	10/5 days	10 m	16 bits	L2A
$r_{Vegetation\ Red\ Edge}$	865 nm	10/5 days	20 m	16 bits	L2A
$r_{SWIR\ 1}$	1610 m	10/5 days	20 m	16 bits	L2A

Source: [59].

Multispectral satellite data were correlated with UAV data. The analyses collected from Sentinel-2A/MSI strictly followed the analysis days according to the treatments (e.g., V4 = 32 DAS; R5 = 47 DAS; R6 = 60 DAS; R8 = 74 DAS; and R9 = 89 DAS). The orbital images and quantitative spectral data were collected from the datasets and open services of the Copernicus Sentinel (Copernicus Data Space Ecosystem) contribution missions (<https://dataspace.copernicus.eu/browser/>—accessed on 31 October 2023), conducted and made available by the European Space Agency (ESA). The satellite analysis days were

the closest possible available, with the dates being 19 July 2021—corresponding to treatment V4; 3 August 2021—corresponding to treatment R5; 16 August 2021—corresponding to treatment R6; 30 August 2021—corresponding to treatment R8; and 14 September 2021—corresponding to treatment R9.

Biophysical Indices (from Sentinel-2A/MSI Satellite)

The estimation of vegetation indices was conducted using multispectral surface reflectance bands obtained from the Sentinel-2A/MSI satellite. These indices serve as sensitive indicators of changes in land cover and use, providing insights into patterns of plant biomass, water availability assessment, water content in vegetation leaves, photosynthetic activity, and vegetation health.

Digital processing of the multispectral images was performed using the Google Earth Engine (GEE) platform/software, which is accessible online at https://earthengine.google.com/ (accessed on 31 October 2023). The GEE offers an open-access platform featuring an integrated library equipped with various mathematical analysis functions, including computational modeling, statistical analyses associated with Geographic Information Systems (GIS), and machine learning operations employing specific algorithms [60]. This platform enables the processing of satellite images and the calculation of different biophysical parameters on the Earth's surface, such as vegetation and water indices.

In this study, methods for calculating vegetation indices from surface reflectance (SR) were employed. A digital processing script was developed and implemented using the Python programming language on the GEE platform, utilizing data from the following collection: GEE ID: Sentinel-2A/MSI—ee.ImageCollection ("COPERNICUS/S2_SR_HARMONIZED"). This collection provides harmonized surface reflectance data from the Sentinel-2A/MSI satellite, facilitating accurate and consistent analysis of vegetation indices over time.

To mitigate the effects of clouds and shadows on image processing, the digital processing script was tailored to incorporate cloud and shadow masks using specific bands from the satellite/sensor data. A key aspect of this approach was the utilization of the Sentinel-2 QA band for cloud masking, where the Sentinel image collection was pre-filtered based on the CLOUDY_PIXEL_PERCENTAGE flag. This ensured that only cloud-free scenes were used for further analysis. The script was customized following the guidelines provided by the rudimentary GEE ID algorithm, which can be accessed at https://code.earthengine.google.com/ef2faa8fb395bed4dec6d8cce4b40e3c?noload=true (accessed on 31 October 2023).

Additionally, to enhance the accuracy of vegetation index estimation (such as the NDVI, NDMI_GAO, and NDWI_GAO), atmospheric correction/calibration factors were applied. These factors, including a multiplication factor of 0.0001 for each multispectral band of the surface reflectance, help adjust the spectral data for atmospheric influences, ensuring more reliable and consistent vegetation index calculations.

The NDVI using sentinel orbital images was estimated for the reason between the difference of the multispectral bands of near-infrared reflectance ($r_{NIR\,1}$) and the red band (r_{RED}) by the sum of the same. The NDVI varies between −1 and 1 and can be determined according to Equation (1) [54–56,61].

$$NDVI = \frac{r_{NIR\,1} - r_{RED}}{r_{NIR\,1} + r_{RED}} \quad (1)$$

where $r_{NIR\,1}$ and r_{RED}, correspond to the reflectance of the multispectral bands of the MSI sensor at the respective central wavelengths (842 nm) and (665 nm), with a spatial resolution of 10 m (Table 2).

The NDMI_GAO using sentinel orbital images was estimated for the reason between the difference of the multispectral bands of near-infrared ($r_{NIR\,2}$) and short-wave infrared

($r_{SWIR\ 1}$) reflectance by the sum of the same. The NDMI_GAO also varies between −1 and 1 and can be determined according to Equation (2) [57].

$$NDMI_{Gao} = \frac{r_{NIR\ 2} - r_{SWIR\ 1}}{r_{NIR\ 2} + r_{SWIR\ 1}} \quad (2)$$

where $r_{NIR\ 2}$ and $r_{SWIR\ 1}$, correspond to the reflectance of the multispectral bands of the MSI sensor with the following central wavelengths (865 and 1610 nm), with a spatial resolution of 20 m, respectively (Table 2).

The NDWI_GAO using sentinel orbital images was estimated for the reason between the difference of the multispectral bands of the green band (r_{GREEN}) and near-infrared band ($r_{NIR\ 1}$) by the sum of the same. The NDMI_GAO also varies between −1 and 1 and can be determined according to Equation (3) [57].

$$NDWI_{Gao} = \frac{r_{GREEN} - r_{NIR\ 1}}{r_{GREEN} + r_{NIR\ 1}} \quad (3)$$

where r_{GREEN} and $r_{NIR\ 2}$, correspond to the reflectance of the multispectral band of the MSI sensor with the following central wavelength (560 nm and 842 nm), with a spatial resolution of 10 m, respectively (Table 2).

The collection of pixel-to-pixel values from the NDVI parameter generated by both the Sentinel-2A/MSI Satellite and the UAV was conducted with the specific objective of analyzing quantitative values in each treatment (V4, R5, R6, R8, and R9). For each treatment, a total of 32 samples were collected for the Sentinel-2A and 32 samples for the UAV, resulting in 160 combinations for each platform. Therefore, considering all treatments during the common bean crop cycle, the overall total of pixel-to-pixel collected samples was 320, with 160 combinations for the Sentinel-2A/MSI and 160 combinations for the UAV. This comprehensive dataset enables a detailed quantitative analysis of the spectral responses throughout the phenological stages of the common bean crop, facilitating the comparison and evaluation of the effectiveness of both satellite and UAV-based remote sensing techniques.

2.6. Statistical Analysis

The data were subjected to analysis of variance and regression at 1 and 5% probability of error (p-value < 0.01; p-value < 0.05). The absence of outliers and the normality of residuals were verified using the Shapiro–Wilk test. To predict the accuracy of the models, the root mean squared error (RMSE) was used, with intuitively coordinated (r) and coordination coordinates (R^2), according to Equations (4), (5), and (6), respectively.

$$RMSE = \sqrt{\frac{\sum_{i=1}^{n}(Yi - Xi)^2}{N}} \quad (4)$$

where N = exception number, Yi = predicted value, and Xi = observed value.

$$r = \frac{\sum(Xi - Xm)(Yi - Ym)}{\sqrt{\sum(Xi - Xm)^2)(\sum(Yi - Ym)^2)}} \quad (5)$$

where Xi = values of variable x, Xm = average of values of x, Yi = values of variable y, and Ym = average of values of y.

$$R^2 = \frac{RSS}{TSS} \quad (6)$$

where RSS = the regression sum of squares and TSS = the total sum of squares.

Models with significant regression coefficients, in addition to higher r and R^2 and lower RMSE values, predict the field results more accurately. RMSE is used to express the precision of the models, taking advantage of the error values in the same dimensions as the

underlying variables [62]. The models were classified according to the magnitude of the dynamics: weak or insignificant ($-0.40 < r < 0.40$), moderate ($0.40 < r < 0.70$; positive or negative values), and strong ($r > 0.70$; positive or negative values) [63,64]. Each plot was inserted into the models, totaling 32 samples for the production variables and 32 samples at each phenological stage for the vegetation indices. For the chlorophyll content, there were 12 samples in V4, R5, and R9, and 24 samples in R6 and R8, considering the treatments that were evaluated in each of these stages.

2.7. Multivariate Statistical Analysis

Furthermore, regarding multispectral data from the UAV and the Sentinel-2A/MSI satellite, specifically analyzing the NDVI biophysical index, multivariate statistical analysis was also applied through principal component analysis (PCA) for the samples of the treatments in the study area, based on the following predictor variables: V4, R5, R6, R8, and R9 (totaling 32 samples for the UAV and 32 samples for the Sentinel-2A/MSI). Based on the principal components (PC), the covariance matrix was obtained to extract the eigenvalues that originate the eigenvectors. It is noteworthy that the eigenvalues are calculated to determine the contribution of each variable to the total variance of the principal components (PC). A high contribution value indicates that the variable is well represented in the PC [65]. To identify the variables that showed correlation, the Kaiser criterion was used, based on eigenvalues above 1, generating components with a relevant amount of information contained in the original data [66]. Principal component correlation analysis was also carried out for all variables, seeking to correlate with the PCA, to highlight possible similarities in the correlations and confirm patterns of changes in the agricultural area.

The cluster analysis (CA) technique was applied between the period of 17 June 2021, and 24 September 2021 to verify the years of greatest similarity based on the NDVI biophysical index. In the study, the hierarchical agglomerative linking method was selected based on the value of the cophenetic correlation coefficient (CCC), establishing a value greater than 0.7 as significant ($CCC \geq 0.7$) [67] and a *p*-value at 99% significance (p–value < 0.01). The methods used and tested in this study were as follows: simple linkage, complete linkage, the inter-group average linkage method, Ward's method, Ward's method (d2), the median method, the centroid method, and the mcquitty method. In this study, the dissimilarity measure used was the square of the Euclidean distance, Equation (7).

$$d_e = \left[\sum_{j=1}^{n}\left(P_{p,\,j} - P_{k,\,j}\right)^2\right]^{0.5} \tag{7}$$

where d_e is the Euclidean distance and $P_{p,j}$ and $P_{k,j}$ are the quantitative variables j of individuals p and k, respectively.

The degree of linkage fit was evaluated using the CCC. This coefficient measures the association between the dissimilarity matrix (phenetic matrix F) and the matrix resulting from the simplification provided by the clustering method (cophenetic matrix c). The CCC is based on Pearson's coefficient (r), which is calculated between the dissimilarity matrix and the matrix resulting from the clustering process [68]. Thus, the larger the r value, the smaller the distortion. In practice, dendrograms with $CCC < 0.7$ indicate the inadequacy of the CA technique [67,68]. The CCC is defined by Equations (8)–(10).

$$CCC = r_{coph} = \frac{\sum_{i=1}^{n-1}\sum_{j>i}^{n}\left(c_{ij} - \bar{c}\right)\left(d_{ij} - \bar{d}\right)}{\sqrt{\sum_{i=1}^{n-1}\sum_{j>i}^{n}\left(c_{ij} - \bar{c}\right)^2}\sqrt{\sum_{i=1}^{n-1}\sum_{j>i}^{n}\left(d_{ij} - \bar{d}\right)^2}} \tag{8}$$

$$\bar{c} = \frac{2}{n(n-1)}\sum_{i=1}^{n-1}\sum_{j>i}^{n} c_{ij} \tag{9}$$

$$\overline{d} = \frac{2}{n(n-1)} \sum_{i=1}^{n-1} \sum_{j>i}^{n} d_{ij} \quad (10)$$

where CCC is the cophenetic correlation coefficient, c_{ij} and d_{ij} are elements of the i-th row and j-th column of the cophenetic and original distance matrix, respectively, and n is the number of elements, where $\overline{c}$ e $\overline{d}$ are the arithmetic means of c_{ij} e d_{ij}, respectively, defined by Equations (9) and (10).

All statistical analyses were performed using R software version 4.2.1 and RStudio version 7.2 [69].

3. Results

In view of the details of the entire context and the methodology proposed and applied in the study, the results section presents the main highlights achieved. The results of the field variables and the different models presented, as well as the results of the UAV and Senitnel-2A/MSI, are accompanied by a series of statistical analyses, from classical to multivariate approaches.

3.1. Spectral Response UAV to Treatments

Among the vegetation indices (IVs), GNDVI and VARI were the most sensitive to different magnesium doses, both adjusted for a quadratic regression model, based on the regression coefficients (Figures 6 and 7). The GNDVI was significant at 1% in R6 and 5% in R9, with coefficients of variation (CV) of 1.43% and 16.03%, respectively. The VARI was significant at 5% at stage R9 and a CV of 2.83%. The other vegetation indices were not significant at the 5% level for any of the treatments, considering all estimates.

The regression curves showed determination coefficients close to 1, with R^2 of 0.80 in R6 and 0.66 in R9 for GNDVI and R^2 of 0.70 for VARI in R9. The IVs GNDVI in R6 and R9 and VARI in R9 presented the highest predicted value in the regression curve at the dose of 500 g ha^{-1}. Values referring to IVs did not differ significantly between magnesium applications at different phenological stages, showing similar results for both and slightly higher means for R6 in the estimates made at R8 and R9.

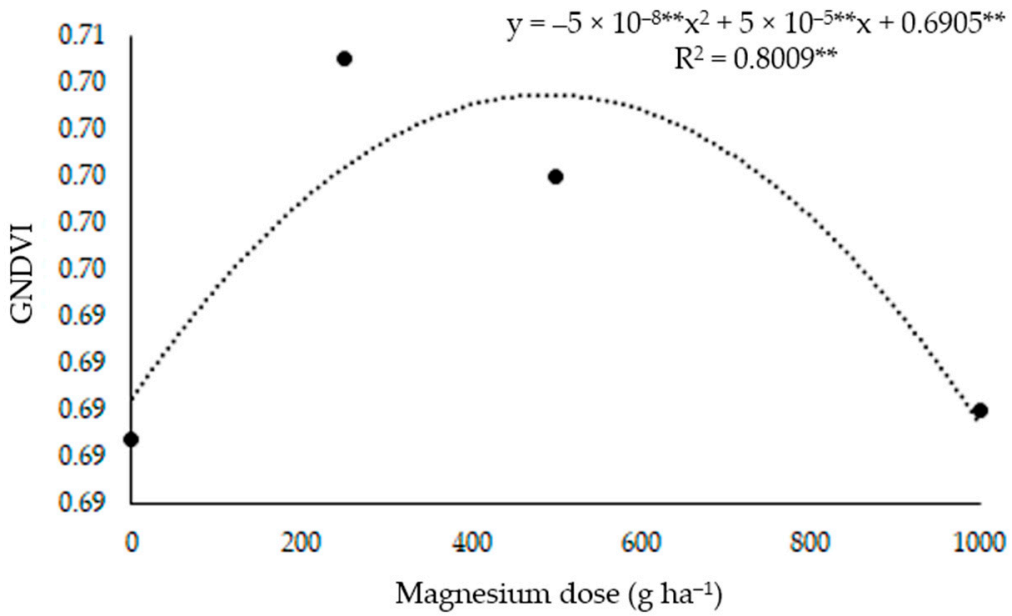


Figure 6. GNDVI as a function of magnesium doses in the R6 phenological stage. ** Significant at 1% probability of error.

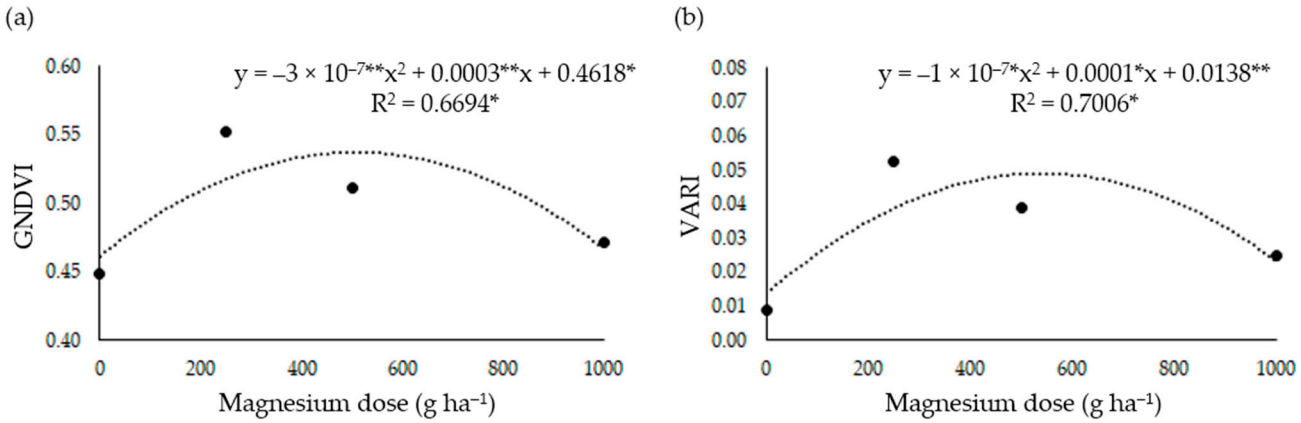


Figure 7. GNDVI (**a**), VARI (**b**) as a function of magnesium doses in the R9 phenological stage. * significant at 5% probability of error, ** Significant at 1% probability of error.

3.2. Prediction of Productive Components

As shown in Table 3, the IVs were better correlated with plant height in R9, where all were followed (p-value < 0.01), the highest skill coordinators, and the lowest RMSE.

Table 3. Correlations between vegetation indices and plant height for different phenological stages.

IVs	Phenological Stage									
	V4		R5		R6		R8		R9	
	r	RMSE	r	RMSE	r	RMSE	r	RMSE	r	RMSE
NDVI	−0.23 ^{ns}	10.6	0.13 ^{ns}	10.8	0.27 ^{ns}	10.5	0.14 ^{ns}	10.8	0.64 **	8.3
GNDVI	−0.04 ^{ns}	10.9	0.17 ^{ns}	10.8	0.52 **	9.4	−0.05 ^{ns}	10.9	0.63 **	8.5
NDRE	−0.31 ^{ns}	10.4	0.16 ^{ns}	10.8	0.43 *	9.9	−0.16 ^{ns}	10.8	0.59 **	8.8
MCARI	−0.25 ^{ns}	10.6	0.24 ^{ns}	10.6	0.29 ^{ns}	10.5	0.40 *	10.0	0.65 **	8.3
LCI	−0.08 ^{ns}	10.9	−0.07 ^{ns}	10.9	0.41 *	10.0	−0.18 ^{ns}	10.8	0.60 **	8.7
SIPI2	−0.38 *	10.1	0.17 ^{ns}	10.8	0.29 ^{ns}	10.5	−0.23 ^{ns}	10.6	−0.47 **	9.7
VARI	0.17 ^{ns}	10.8	0.40 *	10.0	0.57 **	9.0	0.13 ^{ns}	10.9	0.64 **	8.4
TGI	−0.14 ^{ns}	10.8	0.22 ^{ns}	10.7	−0.12 ^{ns}	10.9	0.19 ^{ns}	10.8	0.73 **	7.4

where ** p < 0.01, * p < 0.05, and ns: not significant. r: Pearson's correlation coefficient; RMSE: root mean square error.

The TGI was the only parameter to show a strong correlation (r = 0.73) in R9, with a lower RMSE (7.4 cm), as expressed in the linear regression model, Equation (11). Except for SIPI2, which had the lowest fit and negative correlation (r = −47 and RMSE = 9.7 cm), the other IVs expressed moderate positive correlation (0.59 < r < 0.65; 8.3 < RMSE < 8.8 cm), indicating the viability of IVs in predicting plant height.

$$\text{Plant Heights (cm)} = 403.86\ (x) + 72.21 \quad (11)$$

where x = TGI value.

Only SIPI2 was significant in V4 and VARI was the only one in R5, with correlations in both phenological stages classified as weak (−0.40 < r < 0.40). The VARI and GNDVI IVs were significant at 1% in R6 and NDRE and LCI at 5%, with r values between 0.41 and 0.57 and RMSE between 9 and 10 cm. The MCARI was the only significant IV (p < 0.05) in R8 but with a correlation coefficient of 0.40. The VARI index had the best performance of the others in the phenological stages evaluated preceding the last one, but in R9 it had a lower performance than NDVI, MCARI, and TGI, the latter being the most prominent.

Linear regression models for predicting this variable using MCARI, NDVI, and VARI are described by Equations (12), (13) and (14), respectively.

$$\text{Plant Heights (cm)} = 45.18\ (x) + 68.09 \quad (12)$$

where x = MCARI value.

$$\text{Plant Heights (cm)} = 63.51\ (x) + 64.59 \quad (13)$$

where x = NDVI value.

$$\text{Plant Heights (cm)} = 200.87\ (x) + 94.45 \quad (14)$$

where x = VARI value.

As shown in Table 4, for the number of pods per plant, there were no strong correlations (r > 0.7) with the vegetation indices at any phenological stage, with r values above 0.5 only in R9. There were moderate and significant correlations at 1% in this stage and at 5% in the other stages, except for R5.

Table 4. Correlations between vegetation indices and number of pods per plant for different phenological stages.

IVs	Phenological Stage									
	V4		R5		R6		R8		R9	
	R	RMSE	r	RMSE	r	RMSE	r	RMSE	r	RMSE
NDVI	−0.34 ^{ns}	4.9	−0.07 ^{ns}	5.2	0.22 ^{ns}	5.1	0.14 ^{ns}	5.2	0.62 **	4.1
GNDVI	−0.40 *	4.8	−0.08 ^{ns}	5.2	0.44 *	4.7	0.12 ^{ns}	5.2	0.64 **	4.0
NDRE	−0.28 ^{ns}	5.0	0.27 ^{ns}	5.0	0.23 ^{ns}	5.1	0.08 ^{ns}	5.2	0.61 **	4.1
MCARI	−0.29 ^{ns}	5.0	0.02 ^{ns}	5.2	0.20 ^{ns}	5.1	0.38 *	4.8	0.60 **	4.1
LCI	−0.14 ^{ns}	5.2	0.30 ^{ns}	5.0	0.27 ^{ns}	5.0	0.04 ^{ns}	5.2	0.62 **	4.1
SIPI2	−0.45 **	4.7	−0.18 ^{ns}	5.1	0.39 *	4.8	0.16 ^{ns}	5.2	−0.19 ^{ns}	5.1
VARI	0.05 ^{ns}	5.2	0.18 ^{ns}	5.1	0.25 ^{ns}	5.1	0.06 ^{ns}	5.2	0.53 **	4.3
TGI	−0.10 ^{ns}	5.19	0.05 ^{ns}	5.2	−0.29 ^{ns}	5.0	−0.03 ^{ns}	5.2	0.50 **	4.5

where ** $p < 0.01$, * $p < 0.05$, and ns: not significant. r: Pearson's correlation coefficient; RMSE: root mean square error.

Correlation coefficients above 0.6 were found in R9 for the GNDVI, NDVI, LCI, NDRE, and MCARI indices. The respective linear regression models for predicting this variable are described by Equations (15), (16), (17), (18), and (19), respectively.

$$\text{Number of pods per plant} = 42.587\ (x) + 5.348 \quad (15)$$

where x = GNDVI value.

$$\text{Number of pods per plant} = 29.510\ (x) + 9.676 \quad (16)$$

where x = NDVI value.

$$\text{Number of pods per plant} = 73.58\ (x) + 20.54 \quad (17)$$

where x = LCI value.

$$\text{Number of pods per plant} = 117.5\ (x) + 20.3 \quad (18)$$

where x = NDRE value.

$$\text{Number of pods per plant} = 19.81\ (x) + 12.16 \quad (19)$$

where x = MCARI value.

The vegetation index that best described this variable was the GNDVI, which was significant in V4, R6, and R9, in addition to having the highest correlation coefficient value (r) and the lowest RMSE for the others in R6 and R9. In addition to GNDVI, SIPI2 was significant in V4 and R6, and MCARI in R8. In the stages preceding R9, when the pods had already formed, the correlations were weak or moderate.

Like what was observed in the remaining variables, SIPI2 was the only index with a negative correlation coefficient, and to a lesser extent in R9, being non-significant and classified as weak in predicting the number of variables. The normalized difference indices of the multispectral bands showed better performance, except for SIPI2. The GNDVI, NDVI, NDRE, LCI, and MCARI exhibited correlation coefficients greater than 0.60 and a RMSE between 4 and 4.1, while the VARI and TGI had correlation coefficients below 0.54 and RMSE between 4.3 and 4.5.

There was no strong correlation between the number of grains per pod at any phenological stage (Table 5). Among the significant variables, the correlation was moderate, with r values between 0.36 and 0.68, which indicates little efficiency of the models in predicting this variable under the conditions studied.

Table 5. Correlations between vegetation indices and the number of grains per pod for different phenological stages.

IVs	Phenological Stage									
	V4		R5		R6		R8		R9	
	R	RMSE	r	RMSE	r	RMSE	r	RMSE	r	RMSE
NDVI	0.09 ^{ns}	1.0	0.52 **	0.8	0.47 **	0.9	0.25 ^{ns}	1.0	0.53 **	0.8
GNDVI	0.22 ^{ns}	0.9	0.37 *	0.9	0.52 **	0.8	−0.05 ^{ns}	1.0	0.47 **	0.9
NDRE	−0.11 ^{ns}	1.0	−0.22 ^{ns}	1.0	0.53 **	0.8	−0.01 ^{ns}	1.0	0.40 *	0.9
MCARI	0.04 ^{ns}	1.0	0.56 **	0.8	0.58 **	0.8	0.44 *	0.9	0.57 **	0.8
LCI	−0.10 ^{ns}	1.0	−0.22 ^{ns}	1.0	0.45 **	0.8	−0.03 ^{ns}	1.0	0.45 **	0.9
SIPI2	0.08 ^{ns}	1.0	0.68 **	0.7	0.08 ^{ns}	1.0	−0.14 ^{ns}	1.0	−0.52 **	0.8
VARI	0.29 ^{ns}	0.9	0.66 **	0.7	0.53 **	0.8	0.13 ^{ns}	1.0	0.51 **	0.8
TGI	0.03 ^{ns}	1.0	0.21 ^{ns}	1.0	0.09 ^{ns}	1.0	0.39 *	0.9	0.55 **	0.8

where ** $p < 0.01$, * $p < 0.05$, and ns: not significant. r: Pearson's correlation coefficient; RMSE: root mean square error.

The best fits were obtained for SIPI2 and VARI at R5 (RMSE = 0.7 and r = 0.68 and 0.66, respectively), as shown in Equations (20) and (21) corresponding to the respective linear regression models. The MCARI was the only vegetation index that exhibited a moderate and significant correlation in R8 (r = 0.44), while it was also significant in R5, R6, and R9, with r values between 0.56 and 0.58 and RMSE = 0.8. It can be observed that in the phenological stages V4 and R8, the adjustments were lower than in the others.

$$\text{Number of grains per pod} = 15.516\ (x) - 5.592 \quad (20)$$

where x = SIPI2 value.

$$\text{Number of grains per pod} = 21.32\ (x) + 9.42 \quad (21)$$

where x = VARI value.

The LCI in Stage V4, and the NDVI and SIPI2 in Stage R8, were significant at a 5% probability level ($p < 0.05$) for the linear regressions corresponding to the mass of a thousand grains, with correlation coefficients of −0.42, 0.39, and 0.35, and a RMSE of 18.6, 18.9, and 19.2 g, respectively. Overall, this variable showed only weak correlations across all the estimates. The NDRE showed a significant correlation at 5% for the number of branches per plant, at Stage R5 (r = −0.37). Similarly, to the mass of a thousand grains, this variable

did not show significant correlations in most samples, all of which were classified as weak ($r < 0.40$).

The best correlations and efficiency of the regression models were found for productivity (kg ha^{-1}), for which there was statistical significance for at least one of the indices in all the phenological stages considered (Table 6), in addition to all the significant indices being at 1% significance level in R9.

Table 6. Correlations between vegetation indices and productivity for different phenological stages.

IVs	Phenological Stage									
	V4		R5		R6		R8		R9	
	r	RMSE	r	RMSE	r	RMSE	R	RMSE	r	RMSE
NDVI	−0.34 ^{ns}	538	0.17 ^{ns}	564	0.26 ^{ns}	553	0.30 ^{ns}	544	0.82 **	330
GNDVI	−0.16 ^{ns}	565	0.19 ^{ns}	562	0.58 **	465	0.09 ^{ns}	570	0.78 **	355
NDRE	−0.25 ^{ns}	554	0.20 ^{ns}	560	0.45 **	510	0.03 ^{ns}	571	0.75 **	379
MCARI	−0.37 *	532	0.26 ^{ns}	552	0.36 *	533	0.37 *	530	0.82 **	329
LCI	−0.08 ^{ns}	570	0.22 ^{ns}	558	0.34 ^{ns}	538	−0.02 ^{ns}	572	0.75 **	376
SIPI2	−0.33 ^{ns}	540	0.18 ^{ns}	562	0.24 ^{ns}	555	−0.06 ^{ns}	571	−0.60 **	459
VARI	−0.06 ^{ns}	571	0.49 **	498	0.44 *	512	−0.08 ^{ns}	570	0.67 **	423
TGI	−0.34 ^{ns}	538	0.10 ^{ns}	569	−0.21 ^{ns}	558	0.09 ^{ns}	569	0.74 **	385

where ** $p < 0.01$, * $p < 0.05$, and ns: not significant. R: Pearson's correlation coefficient; RMSE: root mean square error.

VARI and SIPI2 indices evolved significantly, with the latter being inversely proportional to the analyzed variable ($r = -0.60$). The other indices showed strong positive correlation coefficients. The MCARI and NDVI exhibited the best performance with $r = 0.82$ and a RMSE below 331 kg ha^{-1}. Equations (22) and (23) represent the linear regression models of these indices for predicting productivity in this stage. Following that, the GNDVI, LCI, NDRE, and TGI stood out with r values between 0.74 and 0.78 and a RMSE between 355 and 385 kg ha^{-1}. These models are expressed by Equations (24), (25), (26), and (27), respectively.

$$\text{Yield (kg ha}^{-1}) = 2946\ (x) + 936.5 \quad (22)$$

where x = MCARI value.

$$\text{Yield (kg ha}^{-1}) = 4195.4\ (x) + 677.5 \quad (23)$$

where x = NDVI value.

$$\text{Yield (kg ha}^{-1}) = 5620.7\ (x) + 277.4 \quad (24)$$

where x = GNDVI value.

$$\text{Yield (kg ha}^{-1}) = 9753\ (x) + 2279 \quad (25)$$

where x = LCI value.

$$\text{Yield (kg ha}^{-1}) = 15{,}575\ (x) + 2247 \quad (26)$$

where x = NDRE value.

$$\text{Yield (kg ha}^{-1}) = 21{,}159\ (x) + 1571 \quad (27)$$

where x = TGI value.

The indices exhibited negative correlation coefficients at stage V4, indicating an inverse proportion between them and the dependent variable, with only the MCARI showing a significant correlation ($r = -0.37$). Significant correlations were observed for the GNDVI, NDRE, MCARI, and VARI at Stages R5, R6, and R8, all of which were moderate or weak,

ranging between 0.36 and 0.58. During these stages, all plots displayed high vegetative vigor and canopy coverage, leading to peak values for the indices. Several authors have reported the saturation of certain VIs, especially NDVI [70], when they reach higher values.

Overall, MCARI exhibited the highest efficiency in predicting yield, being significant at 5% in treatments V4, R6, and R8, and were significant at 1% in R9. The GNDVI and NDRE were significant at 1% in treatments R6 and R9. With moderate correlations, VARI was significant at R5, R6, and R9.

Figure 8 displays heat maps with Pearson's dynamics matrix depicting all possible combinations of vegetation indices and productive components for each phenological stage.

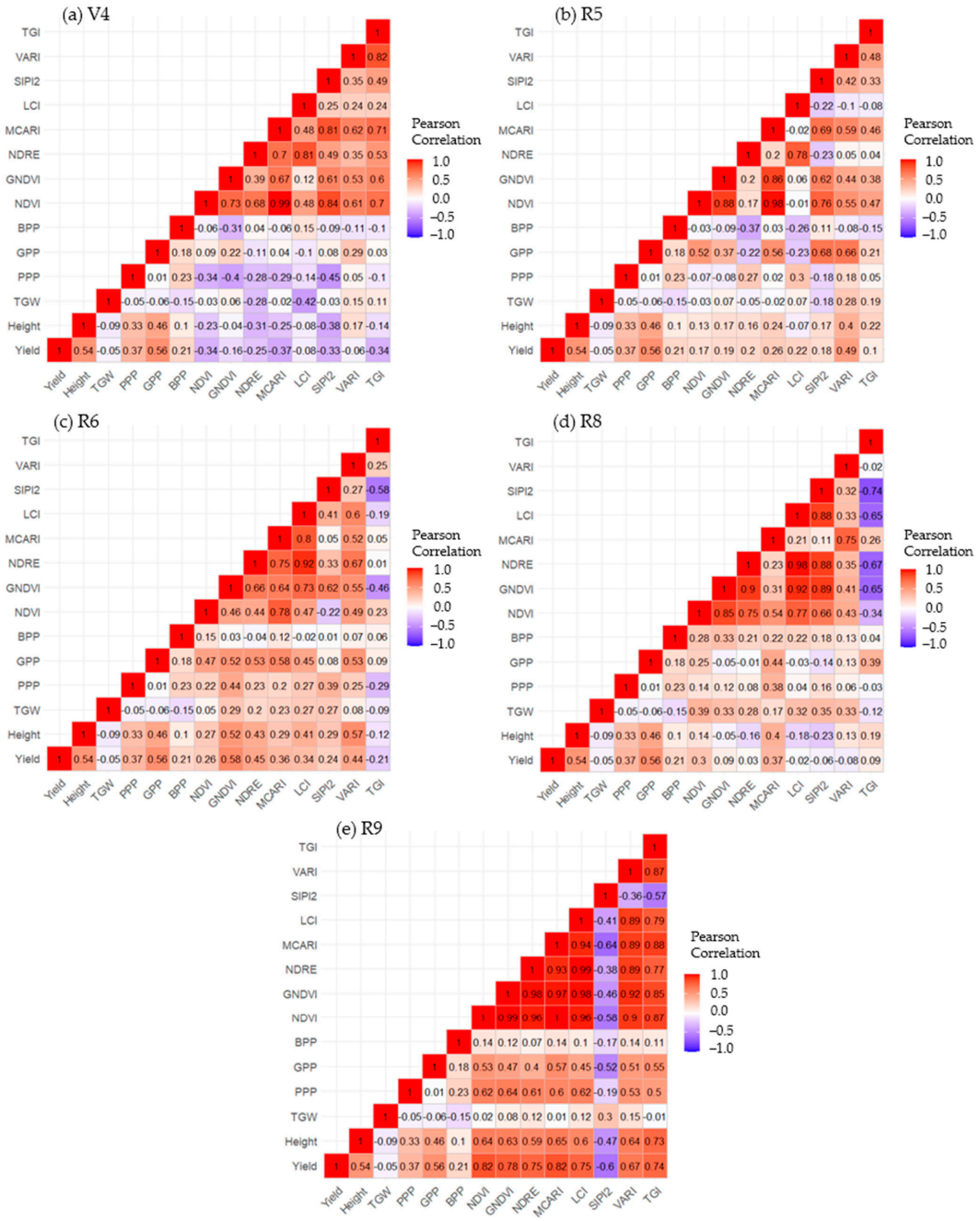


Figure 8. Pearson correlation matrix heat maps for each phenological stage of evaluation—V4 (**a**), R5 (**b**), R6 (**c**), R8 (**d**), and R9 (**e**) indicating the combinations between yield, plant height (Height), thousand grains mass (TGW), pods per plant (PPP), grains per pod (GPP), branches per plant (BPP), and the IVs NDVI, GNDVI, NDRE, MCARI, LCI, SIPI2, VARI and TGI.

Stage V4 presented the weakest correlations, many of which were inverse, between the vegetation indices and other variables, probably due to the strong interference of the soil in the reflectance. The adjustments had a certain progression up to the R6 stage, observed in R8, which can be explained by the uniformity of the vegetative canopy, decrease in the variance between plots, and saturation of some VIs, presenting the maximum values in the entire cycle at this stage.

The best period for predicting the analyzed parameters was at the beginning of R9, when the plants started the process of senescence and grain control, allowing the identification of the best adjustments, with strong automatic coordinators, both between the IVs themselves and between these and other variables (Figure 8e). SIPI2 was the only index with negative r values for all other variables.

Productivity was the variable with the best prediction based on vegetation indices, followed by plant height. The number of pods per plant and grains per pod presents moderate correlations, however with lower comprehension coefficients. At the models' best performance stage (R9), these variables showed strong or moderate correlations, with a lower RMSE and proximity of observed data to those predicted by linear regression (Figure 9). The models for predicting the mass of a thousand grains and the number of branches per plant have not presented a significant correlation.

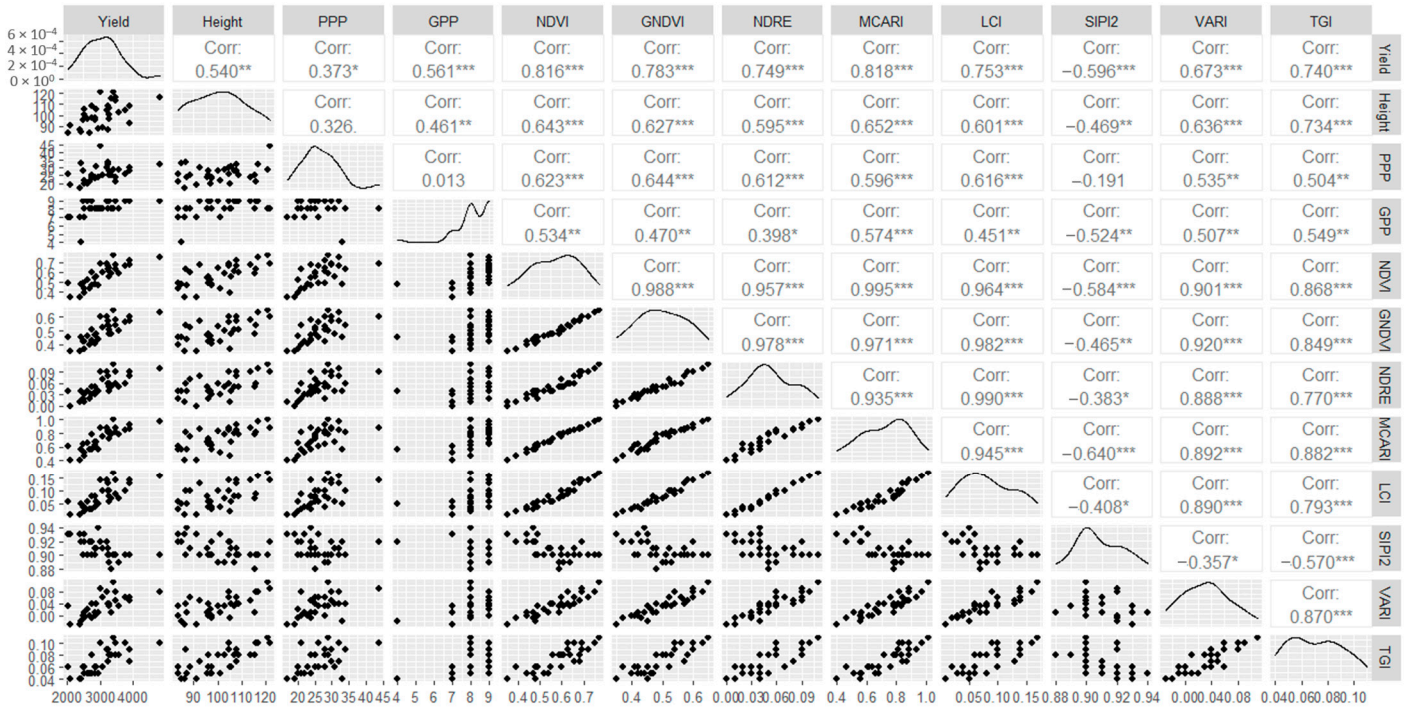


Figure 9. Histogram (diagonal), Pearson correlation (upper-right), and scatter plot (lower-left) between IVs and the following variables: yield, plant height (height), pods per plant (PPP), and grains per pod (GPP). where *** $p < 0.001$, ** $p < 0.01$, * $p < 0.05$.

As depicted in Figure 9, the correlations between IVs with greater statistical significance and r values closer to 1.0 ($0.93 < r < 0.99$) were observed among vegetation indices derived from multispectral bands, except for SIPI2, which displayed an inverse relationship to the others and coefficients of influence smaller than 0.64. IVs derived from RGB images exhibited a strong correlation with each other ($r = 0.87$) and with the NDVI, GNDVI, NDRE, MCARI, and LCI indices ($0.77 < r < 0.92$), with the VARI showing better correlation with these indices than the TGI.

3.3. Prediction of Chlorophyll Content

In Table 7, it can be observed that the VIs did not exhibit a significant difference ($p < 0.05$) concerning chlorophyll content in Stages V4, R6, and R8. However, for Stage R5, there was a moderate and significant correlation at 5% with the MCARI (r = 0.60), VARI (r = 0.61), and TGI (r = 0.57) indices. Among these, the VARI demonstrated the lowest RMSE (16.76), the highest correlation coefficient, and, consequently, the model with the best fit. Figure 10 illustrates the dispersion of the data, the RMSE, the equation, and the coefficient of determination of the line (R^2) for the IVs.

Table 7. Correlations between vegetation indices and chlorophyll content in the different phenological stages.

IVs	Phenological Stage									
	V4		R5		R6		R8		R9	
	r	RMSE	r	RMSE	r	RMSE	r	RMSE	r	RMSE
NDVI	−0.21 ^{ns}	4.35	0.41 ^{ns}	19.31	−0.02 ^{ns}	18.60	0.29 ^{ns}	23.43	0.81 **	10.19
GNDVI	−0.14 ^{ns}	4.35	0.19 ^{ns}	20.80	−0.11 ^{ns}	18.49	0.04 ^{ns}	24.51	0.78 **	10.72
NDRE	0.04 ^{ns}	4.35	0.45 ^{ns}	18.89	−0.05 ^{ns}	18.60	0.12 ^{ns}	24.35	0.79 **	10.58
MCARI	−0.16 ^{ns}	4.35	0.60 *	16.85	0.13 ^{ns}	18.46	0.24 ^{ns}	23.76	0.81 **	10.14
LCI	−0.03 ^{ns}	4.35	0.40 ^{ns}	19.41	0.12 ^{ns}	18.46	0.11 ^{ns}	24.39	0.79 **	10.58
SIPI2	−0.12 ^{ns}	4.35	−0.04 ^{ns}	21.21	−0.005 ^{ns}	18.60	0.14 ^{ns}	24.28	−0.48 ^{ns}	15.16
VARI	−0.17 ^{ns}	4.35	0.61 *	16.76	0.09 ^{ns}	18.52	0.25 ^{ns}	23.68	0.77 **	10.90
TGI	0.15 ^{ns}	4.35	0.57 *	17.32	0.18 ^{ns}	18.27	0.05 ^{ns}	24.49	0.59 *	14.03

where ** $p < 0.01$, * $p < 0.05$, and ns: not significant. r: Pearson's correlation coefficient; RMSE: root mean square error.

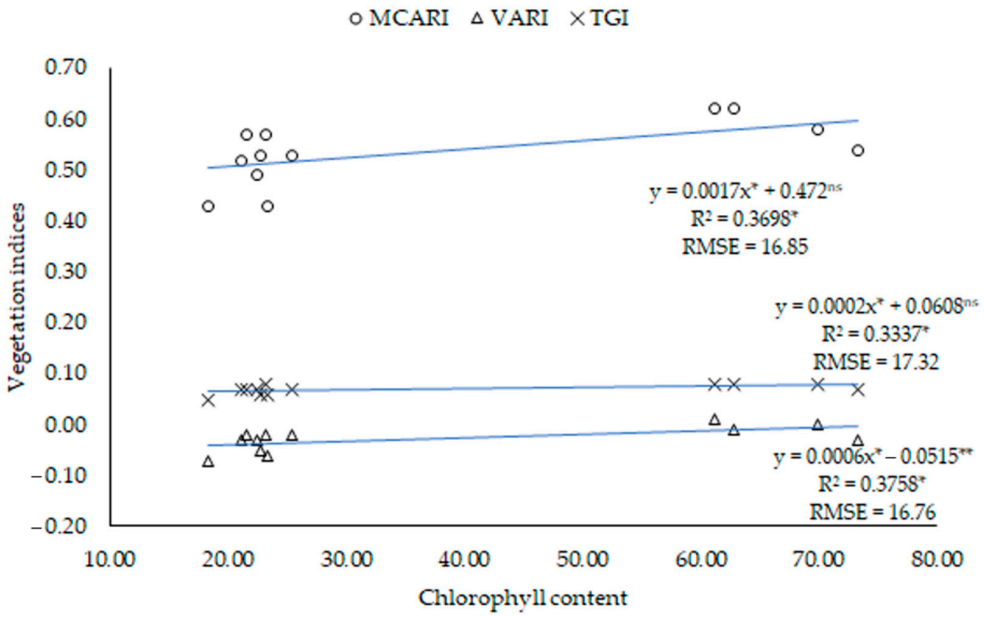


Figure 10. Linear regression between MCARI, VARI, and TGI with SPAD chlorophyll content for the phenological stage R5, where ** $p < 0.01$, * $p < 0.05$, and ns: not significant.

The RMSE values can only be compared within the same column of Table 7 since they are influenced by the magnitude of the values of the variable they describe, and the general averages of the chlorophyll contents were different in the different stages of development of the crop, increasing until reaching the peak at R6 and then declining. This explains the low values for RMSE in V4, for example, even though the correlation coefficient was close to zero for all vegetation indices.

Most of the IVs achieved R^2 values above 0.6 (Figure 11), considering the assessment made at the beginning of the plant senescence period and grain maturation (R9), thus demonstrating good fits of the regression models and, consequently, the high potential of these indices to estimate the chlorophyll content in the common bean crop under the conditions of the present study.

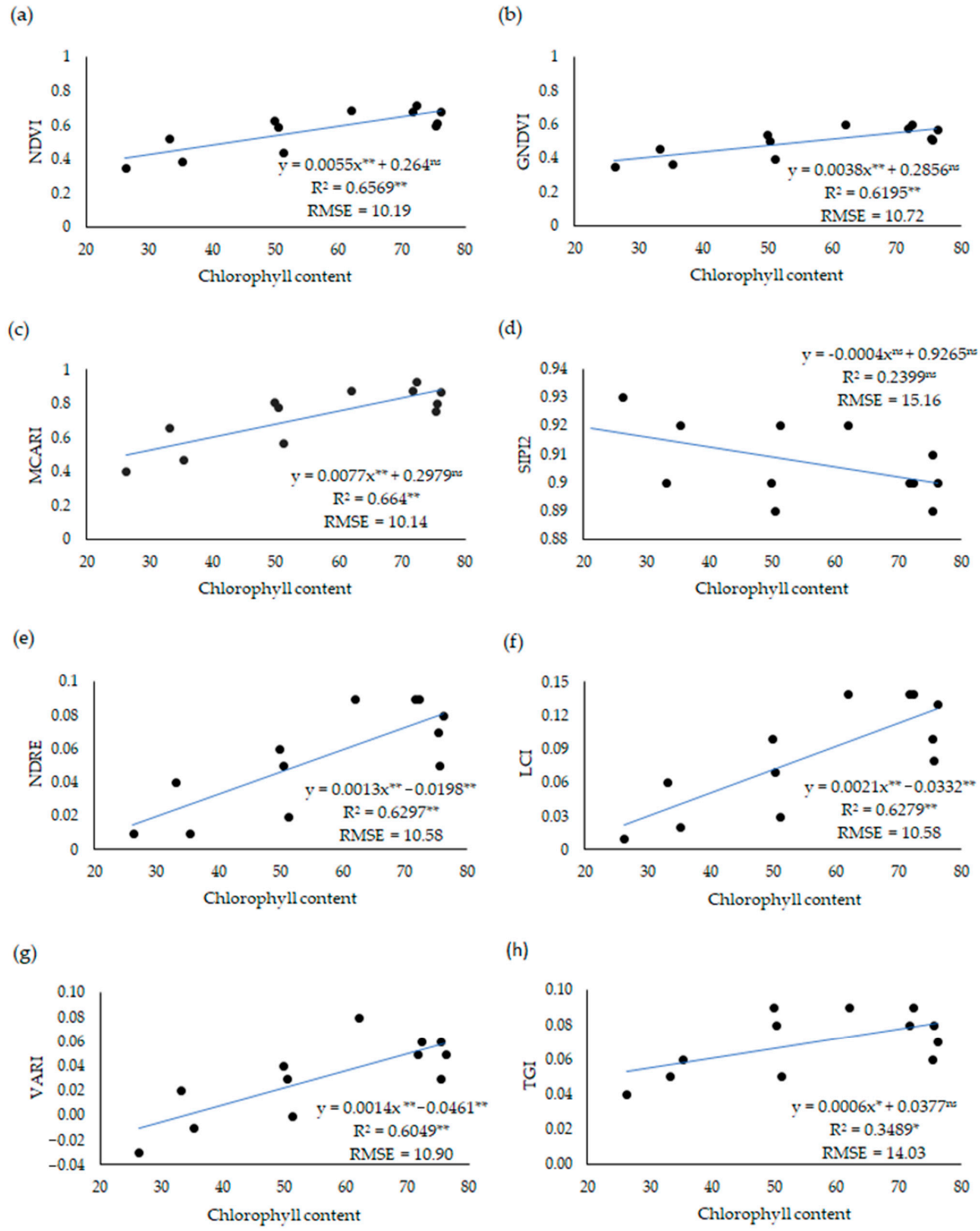


Figure 11. Linear regression plots between chlorophyll content and vegetation indices (NDVI (**a**), GNDVI (**b**), MCARI (**c**), SIPI2 (**d**), NDRE (**e**), LCI (**f**), VARI (**g**), and TGI (**h**)) for the R9 stage. where ** $p < 0.01$, * $p < 0.05$, and ns: not significant.

According to the graphs in Figure 11, in Stage R9, there was a significant interaction with 7 of the 8 vegetation indices tested, showing a strong Pearson correlation and lower RMSE values for MCARI (r = 0.81), NDVI (r = 0.81), NDRE (r = 0.79), LCI (r = 0.79), GNDVI (r = 0.78), and VARI (r = 0.78). Equations (28)–(33) represent the linear regression models of these indices for predicting chlorophyll content. The TGI and SIPI2 exhibited moderate correlation, 0.59 and −0.48, respectively, and the RMSE for both was higher compared to the others (14.03 and 15.16), with SIPI2 being the only non-significant IV.

$$\text{Chlorophyll content (SPAD)} = 85.383\ (x) - 6.049 \quad (28)$$

where x = MCARI value.

$$\text{Chlorophyll content (SPAD)} = 119.48\ (x) - 12.14 \quad (29)$$

where x = NDVI value.

$$\text{Chlorophyll content (SPAD)} = 476.39\ (x) + 30.36 \quad (30)$$

where x = NDRE value.

$$\text{Chlorophyll content (SPAD)} = 300.57\ (x) + 31.02 \quad (31)$$

where x = LCI value.

$$\text{Chlorophyll content (SPAD)} = 163.47\ (x) - 25.17 \quad (32)$$

where x = GNDVI value.

$$\text{Chlorophyll content (SPAD)} = 440.13\ (x) + 42.63 \quad (33)$$

where x = VARI value.

The IVs that exhibited the best performance for the analysis of chlorophyll content were the MCARI and NDVI, with R^2 values of 0.66 and 0.65, respectively. The NDRE, LCI, GNDVI, and VARI also demonstrated prediction coefficients close to these, with R^2 values ranging between 0.60 and 0.63, indicating their high potential for monitoring chlorophyll contents in the vegetative canopy. However, SIPI2 deviated from the other IVs, showing a negative correlation, lower R^2 (0.24), and higher RMSE (15.16). Tisost [71] also obtained negative results between SIPI2 and chlorophyll content, with an R^2 of 0.25.

Regarding the chlorophyll content and productive variables, no significance was obtained in the regressions for the estimates made in V4, R5, R6, and R8. In R9, there were significative interactions with productivity (p-value < 0.01), pods per plant, and grains per pod (p-value < 0.05). Correlations for the number of pods per plant and grains per pod were moderate, with values of r = 0.59 and 0.61, respectively, while for productivity it was strong (r = 0.78). Javed et al. [72] also found positive correlations between chlorophyll concentration and grain yield. Figure 12 allows characterizing the behavior of the relationship between relative chlorophyll content, productivity, and vegetation indices in the phenological stage R9.

The UAV detection of different crop responses based on vegetation indices highlights an important complement to agricultural management and monitoring, particularly considering the challenges in experimental field conditions. Therefore, the combined results provide effective support, primarily for monitoring bean crop growth, facilitating management decisions almost in real time.

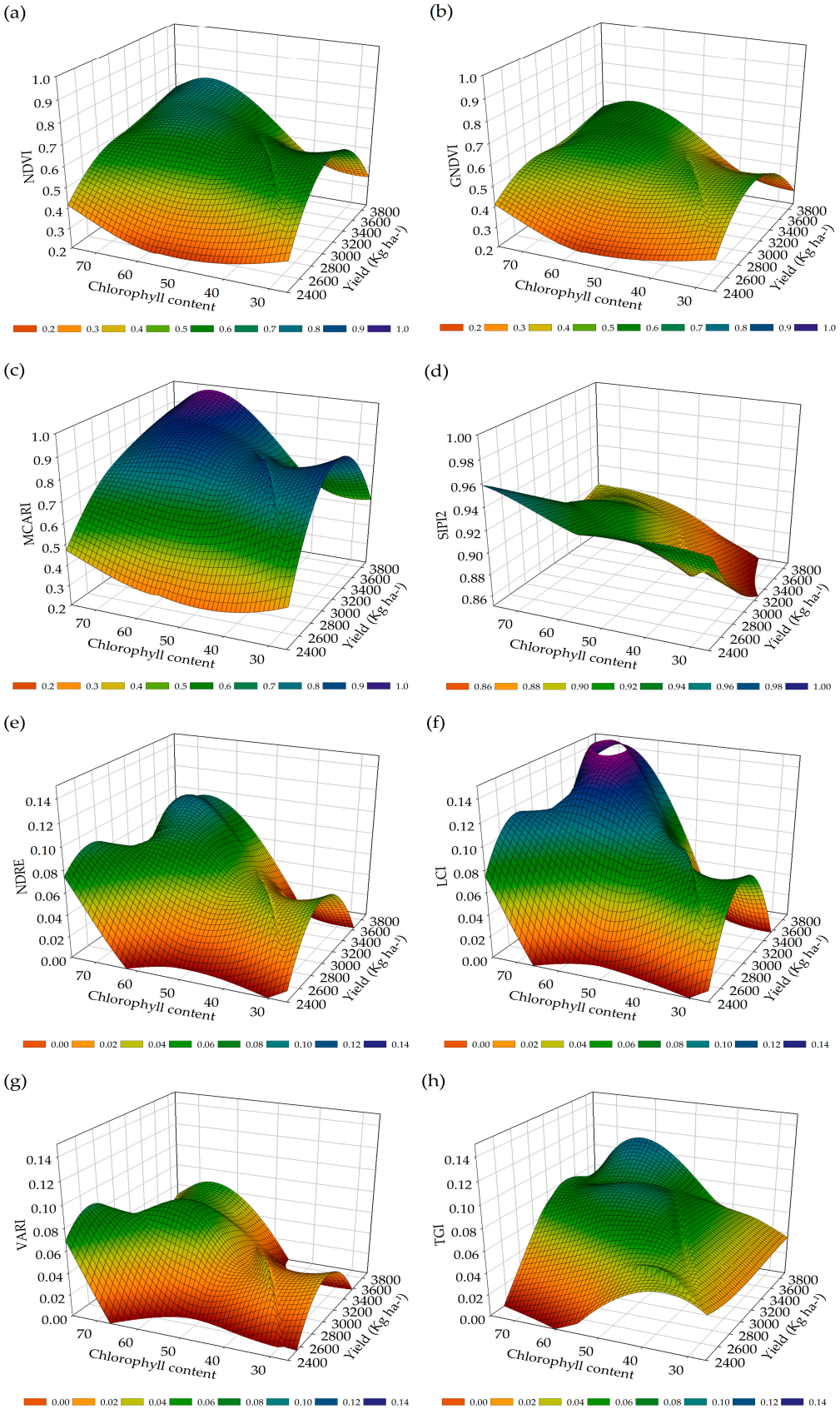


Figure 12. Surface plots of the interaction between productivity, chlorophyll, and the IVs NDVI (**a**), GNDVI (**b**), MCARI (**c**), SIPI2 (**d**), NDRE (**e**), LCI (**f**), VARI (**g**), and TGI (**h**).

3.4. Temporal Variability of Vegetation Indices (IVs)

During the experiment, the IVs showed similar behavior among themselves and followed the growth of the plants and the development of the vegetative canopy (Figure 13). There was an increase in values up to around 45 DAS with maximum peaks between 60 and 90 DAS between the phenological stages R6 and R8, where there was a higher incidence of saturation, the highest for SIPI2 and the lowest for MCARI, which excelled in predicting productivity.

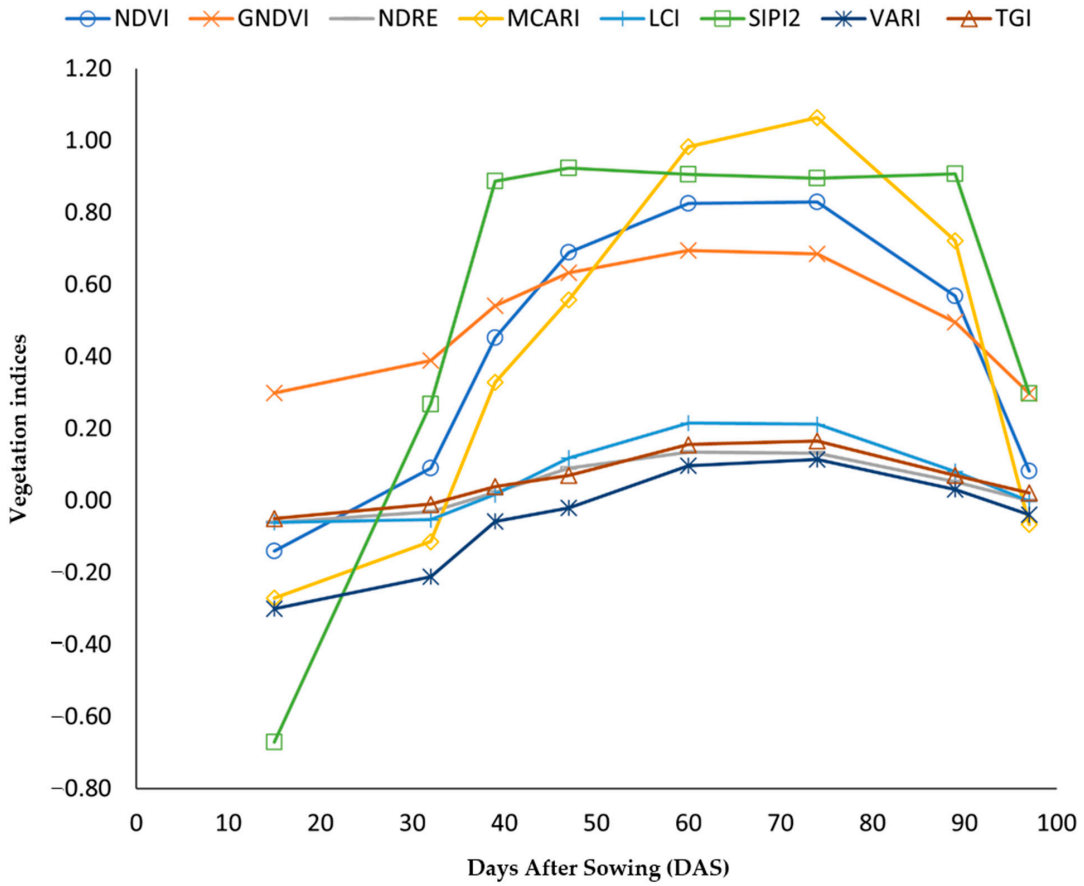


Figure 13. Temporal evolution of vegetation indices as a function of days after sowing (DAS) during the bean cycle.

After the R8 stage, close to 80 DAS, canopy reflectance began to decline, entering the senescence stage, characterized by a decrease in chlorophyll pigments and defoliation. [29]. It is worth noting that the vegetation indices derived from RGB images (VARI and TGI) followed the growth of the crop in a similar way to those that use multispectral bands with higher correlations in the prediction of some variables.

3.5. Satellite Data Analysis (Sentinel-2A/MSI)

In addition to the various analyses, multispectral data from Sentinel-2A/MSI were also applied to the study area, with a spectral resolution of 10 and 20 m, depending on the estimated indices. Thematic maps were generated to visualize the surface estimates of normalized vegetation indices (NDVI, NDMI_GAO, and NDWI_GAO), with values ranging between −1 and 1.

Figure 14 illustrates these thematic maps, which depict various aspects such as photosynthetic activity (RGB), the NDVI, NDMI_GAO, and NDWI_GAO (are presented on the map in columns). The maps correspond to specific dates, namely 19 July 2021 (V4), 3 August 2021 (R5), 16 August 2021 (R6), 30 August 2021 (R8), and 14 September 2021 (R9) (are

presented on the map in lines), representing the progress of days of analysis of treatments from the field experiment. Each line of the map provides a spatial analysis highlighting the respective biophysical indices, offering insights into the vegetation dynamics and health over time during the common bean crop cycle.

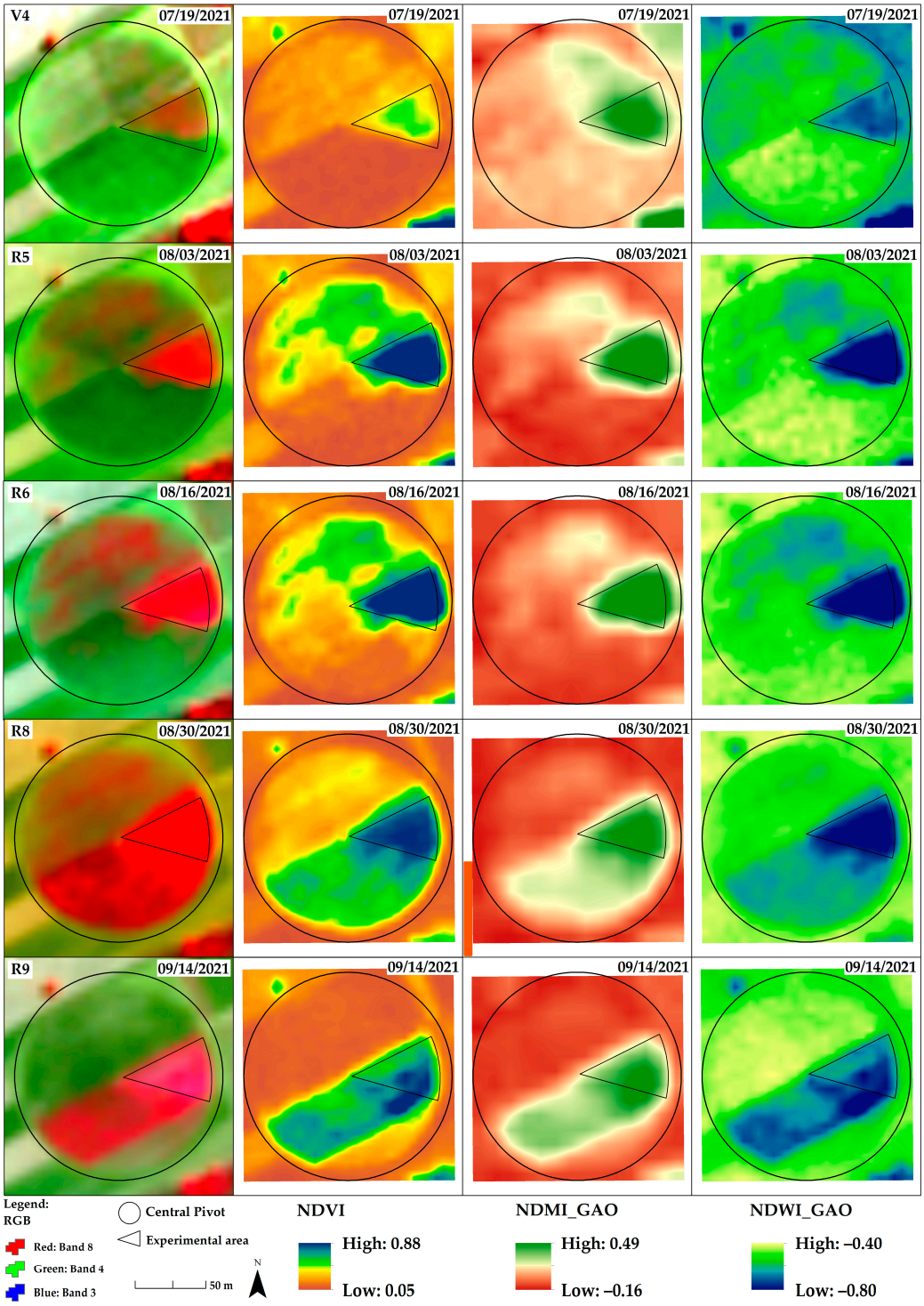


Figure 14. Spatiotemporal distribution of normalized vegetation indices (NDVI, NDMI_GAO, and NDWI_GAO—Sentinel-2A/MSI) in the experimental area with a central pivot for bean cultivation, on 19 July 2021 (V4); 3 August 2021 (R5); 16 August 2021 (R6); 30 August 2021 (R8); and 14 September 2021 (R9).

The use of the infrared multispectral band is important to evaluate photosynthetic and chlorophyll activity, mainly due to the RGB combination of the near-infrared (Band 8), red (Band 4), and green (Band 3) multispectral bands, in addition to the applicability of the indices biophysical. Therefore, throughout the bean crop cycle, the indices showed a significant increase in their density, which presented healthy vegetation, important for adequate development and effective productivity (Figure 14).

In Figure 14, it is observed that the NDVI, NDMI_GAO, and NDWI_GAO have a similar spectral behavior pattern throughout the phenological stages of the bean crop. The vegetation indices used by default vary between −1 and 1. More specifically, the NDVI varied from 0.05 to 0.88, the NDMI_GAO between −0.16 and 0.49, and the NDWI_GAO varied from −0.80 to −0.40. Throughout the bean crop cycle (99 DAS), as it developed, an increase in indices was observed, highlighting the contribution of plant biomass.

The NDVI thematic map was sensitive, as expected, especially on 3 August 2021, 16 August 2021, and 30 August 2021 (corresponding to treatments R5 (47 DAS), R6 (60 DAS), and R8 (74 DAS), respectively), which presented the highest NDVI values, identifying the potential of vegetation green of the bean crop. It is worth highlighting that the spectral explosion in the experimental area with the bean crop occurs, mainly, after the application of the magnesium dose, at 56 days (Figure 14).

The NDVI identified values between 0.40 and 0.50 in the crop growth stage. With the crop in a good state of vegetation, values between 0.60 and 0.70 were observed. According to the results, the bean crop expressed its maximum biomass productivity potential when values from 0.80 were observed, reaching its saturation point (Figure 14).

The NDMI_GAO thematic map was sensitive in identifying the pattern of change in water content in the leaves of the bean crop. It followed spectral behavior like the NDVI, mainly on 16 August 2021 and 30 August 2021. The NDMI_GAO values characterized around zero correspond to crop water stress. The highest positive values of the NDMI_GAO represent leaves without water stress, especially those close to or equal to 1. The NDMI_GAO also efficiently highlighted the moisture distribution conditions in the experimental area (Figure 14).

The NDWI_GAO was also sensitive to the water content present in the leaves of the bean crop. And it followed the same pattern of spectral behavior as the other normalized indices, for all days of analysis and treatments. The spectral behavior of the NDWI_GAO demonstrated healthy vegetation throughout the phenological stages of the bean crop, due to the water present in the leaf canopy (Figure 14).

3.6. Multivariate Analysis: PCA and CCC from Sentinel-2A/MSI x UAV to Treatments (V4, R5, R6, R8, and R9)—Values of the NDVI

Figure 15 highlights the multivariate statistical analysis of principal components—PC1 and PC2 (Figure 15a) and the Pearson correlation (Figure 15b) as a function of the UAV and Sentinel-2A/MSI. The responses are based on the average pixel of the NDVI calculation, according to the variables predicting the phenological stages of the crop (V4, R5, R6, R8, and R9), totaling 32 samples for the UAV and 32 for the Sentinel-2A/MSI. It is noteworthy that according to the criterion established by Kaiser [66], the eigenvalues must be greater than 1 for the components to have a significant information load, which is observed in PC1 and PC2. However, it should be noted that the total variance of the sum of PC1 and PC2 is highly significant, with a total variance of around 88.08% for the experimental area with common beans (Figure 15a).

Between treatments V4 and R9, a significant inversely proportional correlation was observed, with a negative relationship coefficient of −0.8. This response pattern is attributed to the initial phenological stage of the common bean crop (V4) being spectrally confused with the final stage of leaf senescence (R9). During R9, the crop experiences a decrease in chlorophyll pigments and defoliation, resulting in reduced photosynthetic activity, which adversely affects the NDVI values.

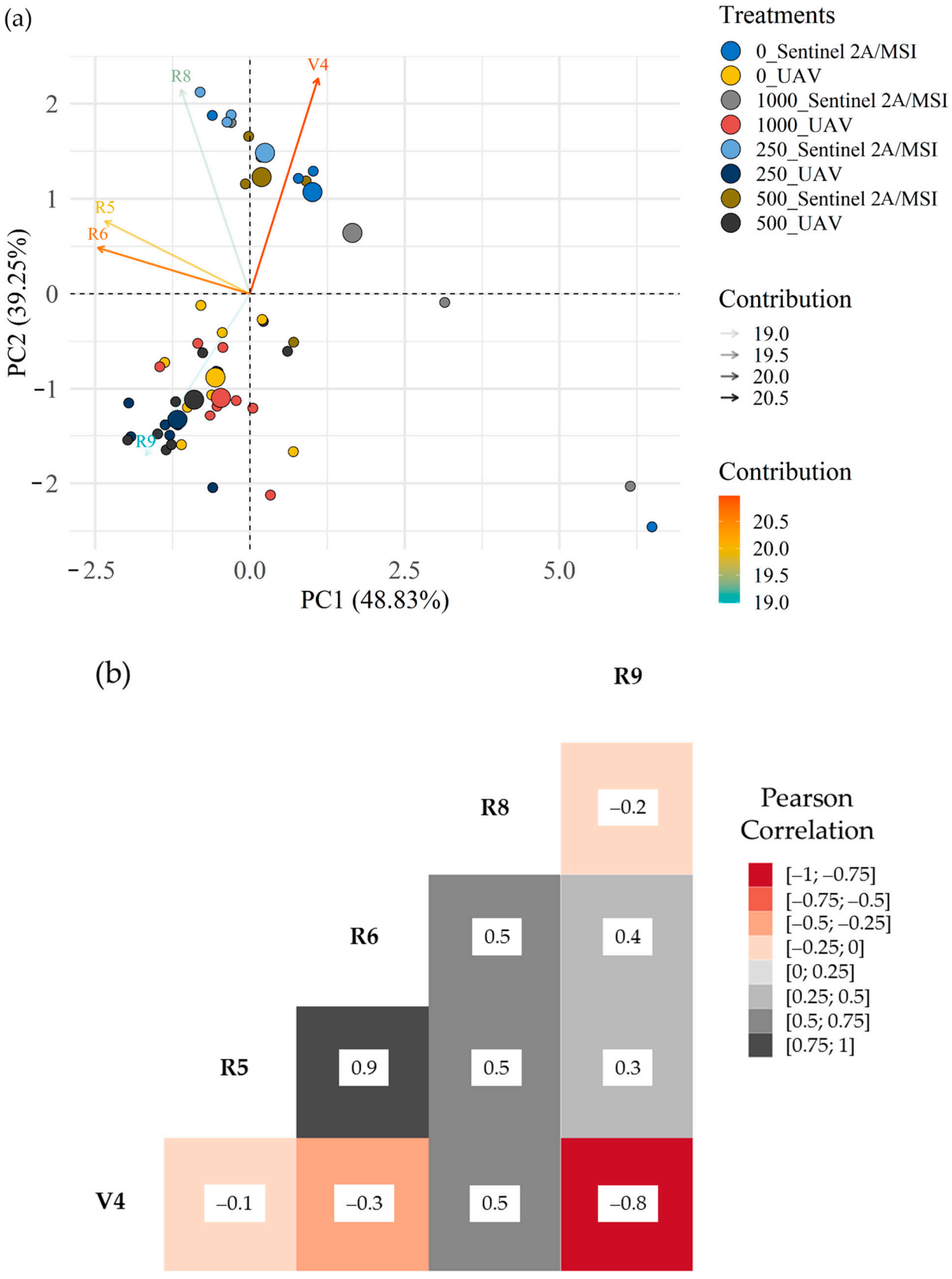


Figure 15. Principal component—PC (**a**) and Pearson correlation (**b**) of the NDVI biophysical index from UAV and Sentinel-2A/MSI in the experimental area with a central pivot for bean cultivation, values of the NDVI on 19 July 2021 (V4); 3 August 2021 (R5); 16 August 2021 (R6); 30 August 2021 (R8); and 14 September 2021 (R9).

On the other hand, in treatments R5 and R6, it was observed a highly significant correlation, indicating a positive relationship coefficient of 0.9. This similar spectral behavior can be attributed to both stages of the common bean crop being in full formation and development, characterized by excellent photosynthetic activity and high chlorophyll content. Additionally, both R5 and R6 showed a good correlation with R8, with a positive relationship coefficient of 0.5. These phenological stages coincide with the application of $MgSO_4$ via foliar spray at 27 and 56 DAS.

Figure 16 illustrates the optimal grouping method for the UAV and Sentinel-2A/MSI samples (four doses of magnesium sulfate—$MgSO_4$: 0, 250, 500, and 1000 g ha^{-1}), determined using the multivariate analysis of the Cophenetic Correlation Coefficient (CCC), which employed the median method. This grouping method demonstrated a satisfactory adjustment with a CCC value of 0.8776 (with a reference value of CCC > 0.70) and a *p*-value of 0.001 (with a reference value of $p < 0.01$), as established in [68]. Thus, this grouping method is recommended for the joint analysis of UAV and satellite data.

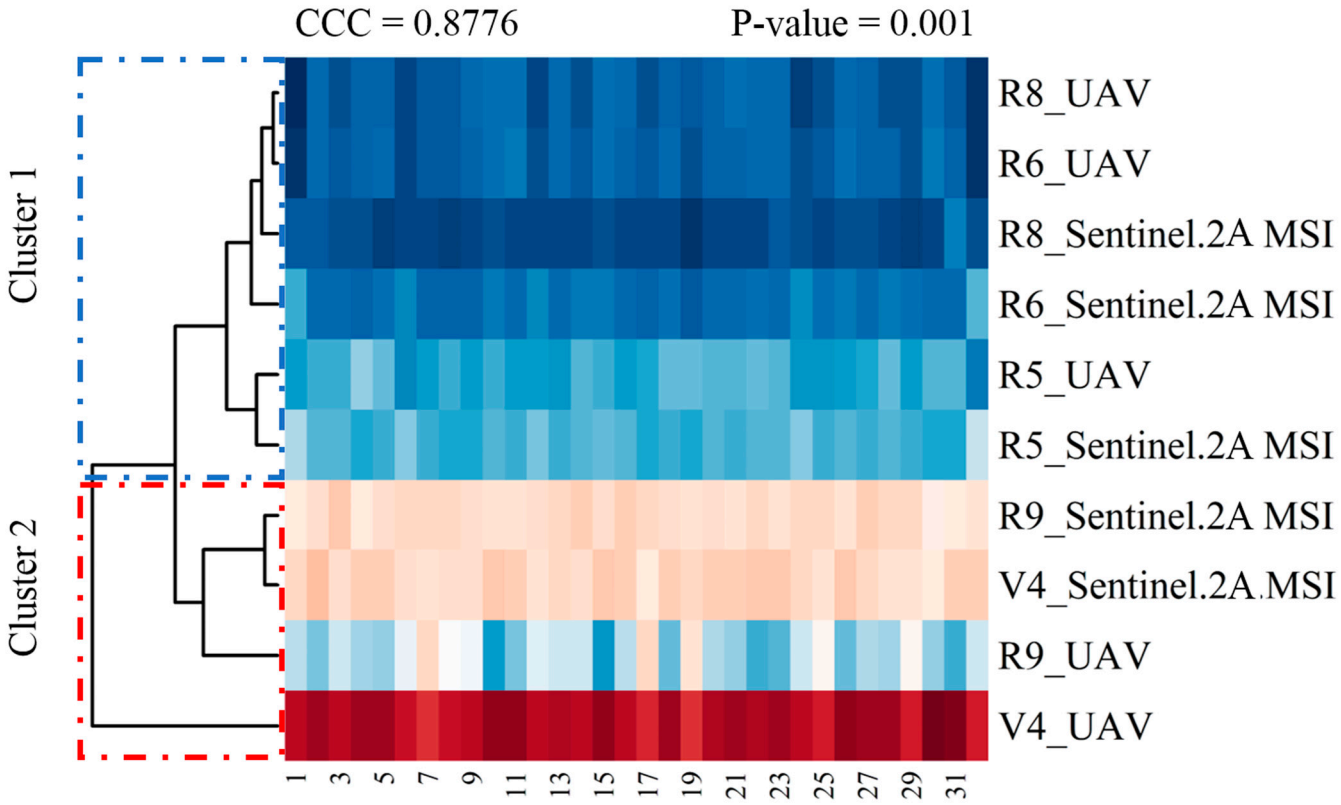


Figure 16. Cluster analysis using the Cophenetic Correlation Coefficient (CCC) of the NDVI biophysical index from UAV and Sentinel-2A/MSI in the experimental area with a central pivot for bean cultivation, values of the NDVI on 19 July 2021 (V4); 3 August 2021 (R5); 16 August 2021 (R6); 30 August 2021 (R8); and 14 September 2021 (R9). Color scale: the red range represents low NDVI values; the blue range represents high NDVI values.

Cluster analysis using the CCC confirmed the formation of two distinct groups (Cluster 1 and 2), exhibiting similar pattern responses within each group (Figure 16). Cluster 1 comprises samples from stages R5, R6, and R8, for both the UAV and the Sentinel-2A/MSI satellite. Within this cluster, the joint correlation between R5_UAV and R5_Sentinel-2A/MSI is noteworthy, indicating no observed distinction in the phenological stage with the use of multispectral geotechnologies. Additionally, the correlation between R6_UAV and R8_UAV is notable, with analysis conducted at 60 and 74 days, respectively. Both also demonstrated a correlation with R8_Sentinel-2A/MSI and R6_Sentinel-2A/MSI (Figure 16). It is important to highlight that UAV and orbital technologies detected more homogeneous pixel

patterns in the experimental area of the common bean, especially when NDVI values were high.

Cluster 2 consists of samples from Stages V4 and R9, for both the UAV and the Sentinel-2A/MSI. Within this cluster, the similarity and correlation pattern of the V4_Sentinel-2A/MSI with R9_Sentinel-2A/MSI stands out, along with their correlation with the V4_UAV and R9_UAV. Despite being different periods representing the beginning (V4) and end (R9) of the common bean crop cycle, they exhibited conditions of low photosynthetic activity and chlorophyll content. Notably, even when the NDVI values are low, Sentinel-2A/MSI tends to homogenize the pixels, which differs from the UAV, highly sensitive in quantitatively detecting differences between V4 and R9, with V4_UAV observing the lowest NDVI values compared to the R9_UAV (Figure 16).

3.7. Multiple Regression Model: Sentinel-2A/MSI x UAV to Treatments (V4, R5, R6, R8, and R9)—Values of the NDVI

Building upon the significant correlations observed in the multivariate analysis, a multiple regression model was developed between the UAV and Sentinel-2A/MSI, based on the NDVI values recorded within the experimental area of the common bean crop at stages V4, R5, R6, R8, and R9 (Figure 17).

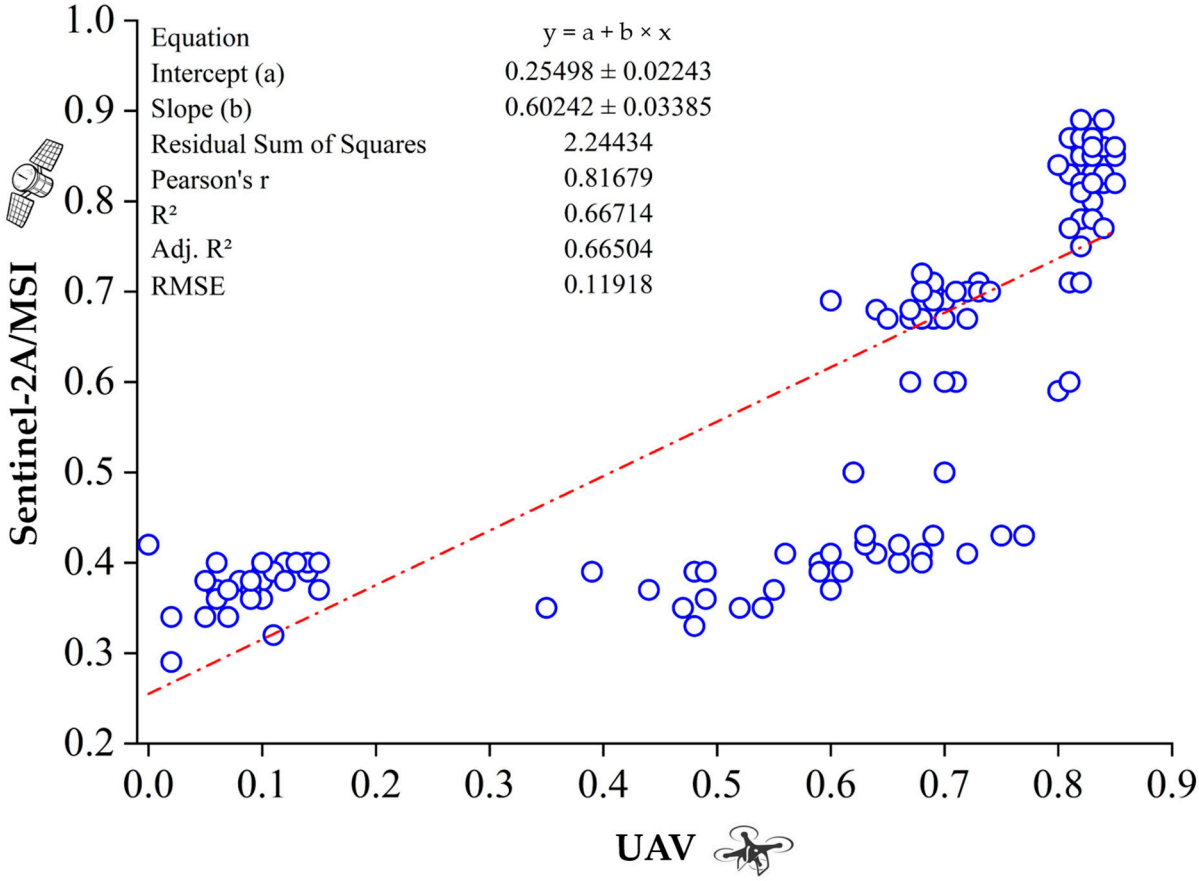


Figure 17. Multiple regression between UAV vs. Sentinel-2A/MSI data applicability in the experimental area with a central pivot for bean cultivation, values of the NDVI on 19 July 2021 (V4); 3 August 2021 (R5); 16 August 2021 (R6); 30 August 2021 (R8); and 14 September 2021 (R9).

The model performed satisfactorily in terms of the descriptive measure of adjustment quality, as evidenced by the high coefficient of determination (R^2), which reached a value of R^2 = 0.667, along with a low root mean square error (RMSE) of 0.12 (Figure 17). The study by Revill et al. [73] with leaf area index (LAI) estimates from the UAV and Sentinel-2 highlighted that the agreement of values increased according to the growth stage of

the wheat crop, with R^2 values varying between 0.32 and 0.75. The authors calibrated the LAI of Sentinel-2 in a single stage, from ground measurements, which showed poor performance, i.e., R^2 value of 0.29 and RMSE of 0.17. However, when looking at the two-stage calibration from the UAV data, the R^2 was 0.88, and the RMSE was 0.08. Govi et al. [3] in the comparison of the NDVI between Sentinel-2 and UAV to eventually explore relationships with agronomic variables in precision agriculture, they presented R^2 values between 0.6 and 0.9.

4. Discussion

With the objective of evaluating the efficiency of vegetation indices determined through multispectral and RGB images, via the UAV and satellite, it is noteworthy that the IVs were effective in predicting the characteristics of biophysical parameters of the common bean crop evaluated in the field, being confirmed through significant statistical correlations. Therefore, indicating more specifically the best vegetation indices through the spectral condition of greater photosynthetic activity during the phenological stages of the crop cycle.

These results provide insights that help us to properly understand the relationship between biophysical parameters collected in the field and multispectral data via the UAV and Sentinel-2A/MSI. The strong correlation of these geotechnologies leads to applications that aim to monitor agronomic variables effectively at a low operational cost.

4.1. Spectral Response UAV to Treatments

The UAV data provided accurate information from the spectral indices, both at the initial and late stages of the bean crop cycle, where the initial stage (V4) of the crop can be easily affected by soil conditions and effects, while in the final stage (R9) a low condition of green vegetation is generally observed, due to the end of the bean crop cycle. However, the responses detected by vegetation indices via the UAV promoted results consistent with the biophysical parameters of the crop evaluated in the field.

The application of magnesium in common beans induced spectral responses in the crop, as evidenced by the significance of the GNDVI and VARI indices at the 5% level (p-value < 0.05) for the magnesium treatment, particularly notable at the R9 stage (R^2 = 0.66 and 0.70 respectively). Additionally, the GNDVI showed significance at the R6 stage (R^2 = 0.80) at a 1% level (p-value < 0.01). The GNDVI, utilizing the green and near-infrared spectrum, is considered a reliable index for indicating canopy health and vigor, being sensitive to changes in chlorophyll concentrations in plants [46,74]. Since magnesium (Mg) is the central atom of the chlorophyll molecule, fluctuations in its levels in the chloroplast regulate the activity of key photosynthetic enzymes [75], Hence, a direct relationship between Mg^{2+} concentration and chlorophyll in plants is expected, which may explain the response of this vegetation index to magnesium application.

Previous research by Sankaran et al. [16] using UAV multispectral images observed that average GNDVI data at 45 (flowering stages), 60 (average pod filling), and 75 (late pod filling) days after sowing (DAS) were significantly correlated with seed yield (r > 0.73) and biomass classification during flowering stages (r from −0.54 to −0.73) and average pod filling (r from −0.52 to −0.73).

This study reveals significant correlations between vegetation indices (IVs), crucial tools in remote sensing, and biophysical parameters of common bean crops. Recent experimental results in productivity prediction through IVs in common beans and other legumes by various authors [5,22,29,76], corroborate the findings of this study, emphasizing that IVs, particularly the MCARI and NDVI, predict productivity and chlorophyll content with the highest magnitude correlations.

It is important to note that vegetation indices can yield improved results with high-resolution imagery, as observed by Sankaran et al. [15], who studied phenotyping, performance, and phenological characteristics of beans using remote sensing techniques based on UAV and satellite. The authors observed a strong relationship between vegetation indices

and biomass (r = −0.55) and seed yield (r = 0.52) during bean pod development stages, emphasizing that the correlation between the NDVI extracted from images decreased with decreasing satellite image resolution.

The vegetation indices (IVs) NDVI, GNDVI, MCARI, LCI, VARI, and the TGI exhibited correlation coefficients above 0.60 and RMSE smaller than 8.7 cm for measuring plant height. Notably, the TGI outperformed the others with a correlation coefficient of 0.73 and RMSE of 7.4 cm. Furthermore, the VARI, another RGB-based index, showed a strong performance (r = 0.63 and RMSE = 8.4 cm), ranking below only two multispectral IVs (the NDVI and MCARI). Ji et al. [77], when assessing the accuracy of models based on RGB and multispectral images for predicting plant height in lima bean (*Vicia faba* L.) crops, reported high results with R^2 = 0.99 and RMSE = 8.05 cm for models derived from RGB images, and R^2 = 0.95 and RMSE = 10.17 cm for models from multispectral images.

Consistent with the main findings of vegetation indices in this study, both UAV and satellite data indicated that treatments R5 (47 DAS), R6 (60 DAS), and R8 (74 DAS) exhibited favorable conditions for high biomass production. Supporting these results, Sankaran et al. [15] emphasized that the NDVI is strongly correlated with performance characteristics such as above-ground biomass, particularly on 60 and 75 DAS.

Moderate or weak correlations were found for the number of pods per plant and grains per pod. The evaluation with the highest presence of significant correlations for pods per plant was at R9, with the GNDVI index performing best (r = 0.64 and RMSE = 4.0). Regarding the number of grains per pod, the most significant prediction was at R5, with the SIPI2 index showing the highest correlation (r = 0.68 and RMSE = 0.7). However, considering that the correlation coefficients for the MCARI were closer to 1.0 than other IVs in the last three phenological stages, with significance for R5 (r = 0.56 and RMSE = 0.8), the MCARI can be considered the vegetation index with the best performance in predicting this variable in the present study.

Based on the magnitude of correlations, none of the IVs proved efficient in predicting the thousand-grain weight and number of branches per plant variables, nor were they significantly correlated with other productive components. There is limited literature addressing the prediction of these variables through remote sensing techniques, indicating the need for further studies on the subject.

Understanding variables related to the physical properties of agricultural products, particularly grains, is crucial for making decisions regarding their conservation, sizing, and equipment maintenance for post-harvest operations. This knowledge helps minimize production costs, enhance competitiveness, and improve product quality [78]. Remote sensing tools offer promising alternatives for acquiring this information in advance, non-destructively, accurately, and swiftly.

The tested indices demonstrated potential for predicting chlorophyll content, particularly based on evaluations conducted during the R9 stage. Spectral data predict chlorophyll content by assessing the spectral reflectance of canopy leaves, which is significantly influenced by changes in chlorophyll concentration and other factors such as canopy architecture, visible spectrum radiation, wavelengths reflected from the ground, and leaf area index [28].

The lower accuracy of vegetation indices (IVs) in predicting chlorophyll during the V4 stage is likely due to interference from soil reflectance. Chlorophyll content primarily affects reflectance in the visible region (RGB), where it regulates much of the spectral response of normal and healthy vegetation. Healthy vegetation absorbs more radiation in the red and blue regions and reflects more in the green regions [79]. Soil reflects most of the light it receives in the red band wavelength (630–690 nm), while chlorophyll absorbs most of the waves it receives in this spectrum. This inverse behavior complicates predictions during vegetative stages, not only for chlorophyll but also for other agronomic parameters.

The improved prediction results observed at the onset of the grain regulatory control period (R9), when plants were undergoing senescence, can be attributed to increased variability in plot reflectance during this period. This increased variability arises from the gradual degradation of chlorophyll and expression of carotenoids on the leaf surface [80,81].

Plots that maintained vegetative vigor for a longer duration exhibited higher average IV values and productivity.

Conversely, during the vegetative period of the crop (V4), prediction model accuracy for variables was generally low. This can be attributed to significant soil reflectance interference, which remained substantial at this stage due to the low vegetative canopy cover. Plants were exposed to numerous biotic and abiotic factors that directly or indirectly influenced yield until the end of the cycle.

The inaccuracies observed in predicting biophysical parameters at the R6 and R8 stages may be explained by the saturation of some IVs during these stages. At these stages, vegetative canopy vigor peaked, and IVs reached their maximum values. For instance, although the NDVI exhibited correlation coefficients above 0.80 for productivity and chlorophyll at R9, it was not significant in other phenological stages, likely due to high soil reflectance in V4 and saturation in subsequent stages with values exceeding 0.70.

Notably, the NDVI and MCARI demonstrated the highest degree of correlation among themselves, with $r > 0.90$ at V4, R5, and R9 stages, standing out in predicting important variables such as productivity and chlorophyll. Other indices derived from multispectral images also exhibited $r > 0.9$ in these stages. Strong correlations were observed between VARI (multispectral) and TGI (RGB) with other IVs, particularly at the R9 stage. This is economically significant as RGB sensors are considerably more affordable than multispectral sensors, making such tools more accessible and promoting the adoption of remote sensing in agriculture.

Currently, there is an increasing trend in precision agriculture toward integrating technologies such as multispectral/hyperspectral/RGB cameras, UAV platforms, and IR yield monitoring results to enable high-capacity data analysis. This utilizes high-resolution geospatial datasets to expand the information network to the field [70]. Identifying areas of low, medium, and high yield at the field level and tracking temporal variations over time facilitate targeted management practices, ultimately enhancing profitability [82].

4.2. Satellite Data Analysis (Sentinel-2A/MSI)

Senitnel-2A/MSI data also provided consistent responses through spectral indices during all phenological stages of the bean crop. In addition to providing large-scale monitoring, the use of this applicability has the advantage of cost-benefit, with quick, effective analysis, and low operating cost. However, unlike UAV data, in the initial stage (V4) of the crop, the data may have been interfered with by soil conditions and effects.

The vegetation indices derived from the multispectral bands of Sentinel-2A/MSI demonstrate a spectral dynamic capable of assisting in the management of bean crops throughout their growth cycle, thereby facilitating proper planning and effective decision making to enhance crop productivity. Soriano-González et al. [19] monitored rice harvesting and estimated yield using Sentinel-2 data, highlighting the rapid changes associated with phenology. The authors also affirm that the Sentinel-2 satellite serves as an excellent tool for agricultural monitoring and crop area management.

The NDVI has proven to be efficient in detecting spectral responses sensitive to green vegetation. Additionally, the NDMI_GAO and NDWI_GAO indicate favorable moisture conditions and water presence conducive to optimal bean crop development. Therefore, it is emphasized that both indices complement each other, and their joint application is recommended to enhance the reliability of spectral results and provide more precise and appropriate diagnoses for agricultural management.

Numerous studies have explored the utilization of remote sensing with satellites to monitor the health, yield, and growth of bean crops [15,34]. The NDVI, for instance, is commonly employed to assess crop health and vegetative density [2,83,84], while water indices such as NDMI_GAO and NDWI_GAO are more specific for evaluating water availability in plants, as highlighted in several studies [57,58,85].

Research findings have demonstrated the effectiveness of the NDVI in monitoring the vegetative development and productivity of beans over time [86,87]. Increasing NDVI

values signify a rise in vegetative cover and crop health, which can be particularly useful for identifying areas experiencing water stress or other growth-related issues [12,85]. Similarly, the NDMI_GAO and NDWI_GAO indices have been utilized to monitor productivity, soil moisture, and water availability for plants. Low NDWI_GAO values may indicate dry conditions or water stress, while higher values may suggest an adequate water supply [56,85].

The choice of various vegetation indices favors the confirmation of the main results. Although they are similar, the normalized vegetation indices, which range from −1 to 1, have specificities that play a complementary role in the analysis of crops. While the NDVI may be more efficient in detecting the green condition of plant health, the NDMI_GAO and NDWI_GAO can more efficiently detect the water content in crops, and diagnosis favors conditions of water deficit.

Using few vegetation indices in certain studies risks greater overestimations and/or underestimations. Therefore, the standardized pattern of vegetation indices helps in more efficient and precise management, based on the different spectral behaviors that confirm and complement each other in most applications.

These studies underscore the utility of remote sensing with the Sentinel-2 satellite in providing valuable insights into the state of bean crops on a large scale and across different growth stages. This information can empower farmers to make informed decisions regarding crop management, optimize resource utilization, and enhance productivity [19,88–90].

4.3. Multivariate Analysis and Multiple Regression Model from Sentinel-2A/MSI x UAV to Treatments (V4, R5, R6, R8, and R9)

In general, the PCA (PC1 = 48.83% and PC2 = 39.25%) reveals that the Sentinel-2A/MSI samples exhibit greater homogeneity, occupying a consistent quantitative behavior pattern in the biplot graph. In contrast, the UAV samples display a more heterogeneous quantitative pattern, indicating greater variability in the data depending on the crop's development stage and the application of $MgSO_4$. Ranjan et al. [34] observed significant relationships between vegetation indices and crop yield, where PCA provided two principal components of the analyzed vegetation indices for the bean crop. For the early growth stage of the crop, the data explained a yield variability of 76% in PC1 and 11% in PC2. In the intermediate stage, it explained 64% (PC1) and 17% in PC2, and in the late stage, it was 69% (PC1) and 16% (PC2).

Several studies recommend the use of CCC analysis because it provides the best grouping method, important for analyzing, for example, biophysical parameter data using the inter-group average linkage method [91], as well as rainfall data using the method of grouping by means [67].

Remote sensing technologies have become increasingly established in agriculture, generating significant interest across various media [92]. The results presented here demonstrate the potential of using remote sensing products, especially vegetation indices, in monitoring common bean crops and predicting parameters of interest. The indices with the best performance were tested for each parameter evaluated within the phenological stages of the crop. Further studies are necessary to better understand the relationships between field variables and spectral responses from UAVs and satellites. Ultimately, a deeper understanding of these relationships has implications for the financial returns of agricultural activities, labor availability, and the utilization of productive inputs.

Regarding the use and applicability of these geotechnologies, some advantages and disadvantages are evident. With UAV, there is the advantage of being able to plan the date, and time, and achieve high spectral resolution mapping of the study area, with minimal atmospheric interference, to determine biophysical parameters such as vegetation indices. However, additional efforts are required with multispectral sensors and calibration processes.

The use of orbital images may encounter interference due to the satellite revisit period, as the Sentinel-2A/MSI has a defined pass time (5 days) for imaging the surface over

time. Although it offers an efficient spectral resolution of 10 m, as evidenced in the detection of NDVI values, difficulties may arise due to the need to observe specific periods corresponding to the phenological stages of the crop, as indicated in the research by [93], which studied crop distribution using UAV technologies and Sentinel-2A data and found better results for crop classification from the fusion of UAV and satellite data.

Although the applicability of multispectral UAV and Sentinel-2A/MSI data presented important results, more studies are needed to better understand field variables and spectral responses. A main recommendation in the case of satellite images is to improve the spectral resolution of the image.

5. Conclusions

This study successfully achieved its objective of determining and evaluating the behavior of biophysical parameters and biophysical indices, generating sensitive indicators for agricultural monitoring using geotechnologies, specifically UAV and Satellite data, along with field experimental data. These technologies effectively detected spectral information, allowing for the presentation of various dynamics throughout the common bean crop cycle. Both UAV and satellite technologies demonstrated their specific strengths, identifying promising indices for agriculture with satisfactory results, and showing good precision.

In analyzing UAV data, the NDVI and MCARI vegetation indices exhibited the strongest correlations with productivity and chlorophyll, followed by the GNDVI, NDRE, and LCI, which also displayed robust correlations. The VARI showed a strong correlation with chlorophyll, while the TGI maintained a strong correlation with productivity and plant height. Other indices showed moderate or weak correlations, and the remaining variables did not exhibit strong correlations with vegetation indices. Indices derived from RGB images showed results comparable to those from multispectral images, with strong correlation coefficients observed for the VARI and TGI, indicating their efficacy in performance evaluation.

The adjusted equation using the GNDVI and VARI indices indicated that the optimal magnesium dose applied through foliar spraying was 500 g ha^{-1}. Additionally, the beginning of the R9 phenological stage was identified as the optimal period for determining the biophysical parameters of the common bean crop.

Furthermore, the normalized indices determined by Sentinel-2A/MSI also demonstrated significant sensitivity in detecting patterns of change throughout the common bean experiment. The 10 m sensor resolution of Sentinel-2A/MSI proved to be highly accurate for agricultural monitoring through biophysical indices, being the best source of information on a large spatial scale in a practical and quick way, with the advantage of being free.

The combined use of UAV and Sentinel-2A/MSI technologies showed good correlation and effectiveness for spectral monitoring during the common bean crop cycle, offering a cost-effective advantage and providing a higher level of technological and biophysical information on common bean crops.

Multivariate PC and CCC analysis validated the precision and accuracy of UAV technology, particularly emphasizing its sensitivity across different stages of common beans. Among this analysis, the V4_UAV stage of the CCC analysis represented the efficiency of UAV multispectral technology most prominently, especially when compared to Sentinel-2A/MSI orbital geotechnology, which tended to homogenize pixel values in the study area. The UAV provides image acquisition almost in real time, helping to present an immediate solution to problems generally faced by the canopy of agricultural crops, and also with a relatively low operating cost due to today being much more conventional equipment.

Author Contributions: Conceptualization, L.E.V.d.C., H.F.E.d.O. and L.R.A.J.; methodology, L.E.V.d.C., H.F.E.d.O., J.A.O.S.S., C.M.S. and L.R.A.J.; software, L.E.V.d.C.; validation, L.E.V.d.C., H.F.E.d.O. and L.R.A.J.; software, L.E.V.d.C., J.A.O.S.S., M.V.d.S. and J.L.B.d.S.; validation, L.E.V.d.C., H.F.E.d.O., J.L.B.d.S. and L.R.A.J.; formal analysis, L.E.V.d.C., H.F.E.d.O., L.C.F., J.L.B.d.S., J.A.O.S.S., M.V.d.S., C.M.S., J.F.d.O.J., V.S.d.S., P.R.G., M.M. and L.R.A.J.; investigation, L.E.V.d.C., H.F.E.d.O., J.L.B.d.S.,

M.V.d.S., M.M. and C.M.S.; resources, H.F.E.d.O., J.F.d.O.J., V.S.d.S., P.R.G. and C.M.S.; data curation, L.E.V.d.C., L.C.F., H.F.E.d.O., J.A.O.S.S., M.M. and C.M.S.; writing—original draft preparation, L.E.V.d.C. and H.F.E.d.O.; writing—review and editing, L.E.V.d.C., H.F.E.d.O., L.C.F., M.M., J.L.B.d.S., M.V.d.S., C.M.S., J.A.O.S.S., J.F.d.O.J., V.S.d.S., P.R.G. and L.R.A.J.; visualization, C.M.S., L.E.V.d.C., L.C.F., J.A.O.S.S., H.F.E.d.O., J.L.B.d.S., M.M., M.V.d.S. and L.R.A.J.; supervision, H.F.E.d.O. and C.M.S.; project administration, H.F.E.d.O.; funding acquisition, H.F.E.d.O. All authors have read and agreed to the published version of the manuscript.

Funding: This research was funded by the Goiano Federal Institute.

Data Availability Statement: Sentinel-2A/MSI data presented in this study are available on open services of the Copernicus Sentinel (Copernicus Data Space Ecosystem) contribution missions (<https://dataspace.copernicus.eu/browser/>—accessed on 31 October 2023), conducted by the European Space Agency (ESA). Other data presented in this study are available on request from the first author.

Acknowledgments: The authors extend their gratitude to the Goiano Federal Institute for their assistance with research and publication expenses. To the Cerrado Irrigation Graduate Program for research support. The authors also would like to express sincere appreciation to Copernicus Sentinel contribution missions for the availability of Senitnel-2A/MSI images, and also to Google for providing availability of the Google Earth Engine (GEE), cloud digital processing software. Furthermore, we would also like to thank the anonymous reviewers and the Editors for their insightful comments, which substantially increased the impact of this study.

Conflicts of Interest: The authors declare no conflicts of interest.

References

1. Titolo, A. Use of Time-Series NDWI to Monitor Emerging Archaeological Sites: Case Studies from Iraqi Artificial Reservoirs. *Remote Sens.* **2021**, *13*, 786. [CrossRef]
2. Stamford, J.D.; Vialet-Chabrand, S.; Cameron, I.; Lawson, T. Development of an Accurate Low Cost NDVI Imaging System for Assessing Plant Health. *Plant Methods* **2023**, *19*, 9. [CrossRef] [PubMed]
3. Govi, D.; Pappalardo, S.E.; de Marchi, M.; Meggio, F. From Space to Field: Combining Satellite, UAV and Agronomic Data in an Open-Source Methodology for the Validation of NDVI Maps in Precision Viticulture. *Remote Sens.* **2024**, *16*, 735. [CrossRef]
4. Széles, A.; Huzsvai, L.; Mohammed, S.; Nyéki, A.; Zagyi, P.; Horváth, É.; Simon, K.; Arshad, S.; Tamás, A. Precision Agricultural Technology for Advanced Monitoring of Maize Yield under Different Fertilization and Irrigation Regimes: A Case Study in Eastern Hungary (Debrecen). *J. Agric. Food Res.* **2024**, *15*, 100967. [CrossRef]
5. de Sandrini, F.O.T.; Leal, F.T.; Coelho, A.P.; Lemos, L.B.; Rosalen, D.L. Vegetation Indices in the Estimation of Common Bean Yield Cultivated under Nitrogen Rates. *Rev. Bras. Cienc. Agrar.* **2019**, *14*, 2–9. [CrossRef]
6. Kganyago, M.; Adjorlolo, C.; Mhangara, P.; Tsoeleng, L. Optical Remote Sensing of Crop Biophysical and Biochemical Parameters: An Overview of Advances in Sensor Technologies and Machine Learning Algorithms for Precision Agriculture. *Comput. Electron. Agric.* **2024**, *218*, 108730. [CrossRef]
7. Mosleh, M.K.; Hassan, Q.K.; Chowdhury, E.H. Application of Remote Sensors in Mapping Rice Area and Forecasting Its Production: A Review. *Sensors* **2015**, *15*, 769–791. [CrossRef] [PubMed]
8. Jiang, J.; Atkinson, P.M.; Chen, C.; Cao, Q.; Tian, Y.; Zhu, Y.; Liu, X.; Cao, W. Combining UAV and Sentinel-2 Satellite Multi-Spectral Images to Diagnose Crop Growth and N Status in Winter Wheat at the County Scale. *Field Crops Res.* **2023**, *294*, 108860. [CrossRef]
9. Sahoo, R.N.; Rejith, R.G.; Gakhar, S.; Ranjan, R.; Meena, M.C.; Dey, A.; Mukherjee, J.; Dhakar, R.; Meena, A.; Daas, A.; et al. Drone Remote Sensing of Wheat N Using Hyperspectral Sensor and Machine Learning. *Precis. Agric.* **2024**, *25*, 704–728. [CrossRef]
10. Zhang, L.; Zhang, H.; Niu, Y.; Han, W. Mapping Maize Water Stress Based on UAV Multispectral Remote Sensing. *Remote Sens.* **2019**, *11*, 605. [CrossRef]
11. Shao, G.; Han, W.; Zhang, H.; Zhang, L.; Wang, Y.; Zhang, Y. Prediction of Maize Crop Coefficient from UAV Multisensor Remote Sensing Using Machine Learning Methods. *Agric. Water Manag.* **2023**, *276*, 108064. [CrossRef]
12. Saravia, D.; Valqui-Valqui, L.; Salazar, W.; Quille-Mamani, J.; Barboza, E.; Porras-Jorge, R.; Injante, P.; Arbizu, C.I. Yield Prediction of Four Bean (*Phaseolus Vulgaris*) Cultivars Using Vegetation Indices Based on Multispectral Images from UAV in an Arid Zone of Peru. *Drones* **2023**, *7*, 325. [CrossRef]
13. Killeen, P.; Kiringa, I.; Yeap, T.; Branco, P. Corn Grain Yield Prediction Using UAV-Based High Spatiotemporal Resolution Imagery, Machine Learning, and Spatial Cross-Validation. *Remote Sens.* **2024**, *16*, 683. [CrossRef]
14. Agência Nacional de Aviação Civil (ANAC). Regulamento Brasileiro Da Aviação Civil (RBAC-E) Nº 94. *Diário Oficial União* **2021**, *117*, 1–34.
15. Sankaran, S.; Quirós, J.J.; Miklas, P.N. Unmanned Aerial System and Satellite-Based High Resolution Imagery for High-Throughput Phenotyping in Dry Bean. *Comput. Electron. Agric.* **2019**, *165*, 104965. [CrossRef]
16. Sankaran, S.; Zhou, J.; Khot, L.R.; Trapp, J.J.; Mndolwa, E.; Miklas, P.N. High-Throughput Field Phenotyping in Dry Bean Using Small Unmanned Aerial Vehicle Based Multispectral Imagery. *Comput. Electron. Agric.* **2018**, *151*, 84–92. [CrossRef]

17. Andrade, R.G. Uso de Veículo Aéreo Não Tripulado (VANT). No Monitoramento dos Estádios de Desenvolvimento da Cultura Do Milho. In *Embrapa Gado de Leite-Capítulo em Livro Técnico (INFOTECA-E)*; da Silva, H.C., Ed.; Engenharia Sanitária e Ambiental, Atena Editora: Ponta Grossa, Brazil, 2019; pp. 225–234.
18. Javornik, T.; Carović-Stanko, K.; Gunjača, J.; Vidak, M.; Lazarević, B. Monitoring Drought Stress in Common Bean Using Chlorophyll Fluorescence and Multispectral Imaging. *Plants* **2023**, *12*, 1386. [CrossRef]
19. Soriano-González, J.; Angelats, E.; Martínez-Eixarch, M.; Alcaraz, C. Monitoring Rice Crop and Yield Estimation with Sentinel-2 Data. *Field Crops Res.* **2022**, *281*, 108507. [CrossRef]
20. Candiago, S.; Remondino, F.; De Giglio, M.; Dubbini, M.; Gattelli, M. Evaluating Multispectral Images and Vegetation Indices for Precision Farming Applications from UAV Images. *Remote Sens.* **2015**, *7*, 4026–4047. [CrossRef]
21. de Souza, A.E.S.; Barbosa Júnior, M.R.; de Almeida Moreira, B.R.; da Silva, R.P.; Lemos, L.B. UAV Multispectral Data: A Reliable Approach for Managing Phosphate-Solubilizing Bacteria in Common Bean. *Agronomy* **2022**, *12*, 2284. [CrossRef]
22. Plaza, J.; Criado, M.; Sánchez, N.; Pérez-Sánchez, R.; Palacios, C.; Charfolé, F. UAV Multispectral Imaging Potential to Monitor and Predict Agronomic Characteristics of Different Forage Associations. *Agronomy* **2021**, *11*, 1697. [CrossRef]
23. Atzberger, C. Advances in Remote Sensing of Agriculture: Context Description, Existing Operational Monitoring Systems and Major Information Needs. *Remote Sens.* **2013**, *5*, 949–981. [CrossRef]
24. Andrade, S.M.; Teodoro, L.P.R.; Baio, F.H.R.; Campos, C.N.S.; Roque, C.G.; da Silva, C.A., Jr.; Coradi, P.C.; Teodoro, P.E. High-Throughput Phenotyping of Soybean Genotypes under Base Saturation Stress Conditions. *J. Agron. Crop Sci.* **2021**, *207*, 814–822. [CrossRef]
25. Clevers, J.G.P.W. Application of a Weighted Infrared-Red Vegetation Index for Estimating Leaf Area Index by Correcting for Soil Moisture. *Remote Sens. Environ.* **1989**, *29*, 25–37. [CrossRef]
26. Tahir, N.; Li, J. Hyperspectral Remote Estimation of Leaf Nitrogen Content of Hyperspectral Remote Estimation of Leaf Nitrogen Content. *Sci. Int.* **2015**, *27*, 1689–1691.
27. Naveed Tahir, M.; Lan, Y.; Zhang, Y.; Wang, Y.; Nawaz, F.; Arslan Ahmed Shah, M.; Gulzar, A.; Shahid Qureshi, W.; Manshoor Naqvi, S.; Zaigham Abbas Naqvi, S. Real Time Estimation of Leaf Area Index and Groundnut Yield Using Multispectral UAV. *Int. J. Precis. Agric. Aviat.* **2018**, *1*, 1–6. [CrossRef]
28. Qi, H.; Zhu, B.; Kong, L.; Yang, W.; Zou, J.; Lan, Y.; Zhang, L. Hyperspectral Inversion Model of Chlorophyll Content in Peanut Leaves. *Appl. Sci.* **2020**, *10*, 2259. [CrossRef]
29. Daughtry, C.S.T.; Gallo, K.P.; Bauer, M.E. Spectral Estimates of Solar Radiation Intercepted by Corn Canopies. *Agron. J.* **1983**, *75*, 527–531. [CrossRef]
30. Jewan, S.Y.Y.; Pagay, V.; Billa, L.; Tyerman, S.D.; Gautam, D.; Sparkes, D.; Chai, H.H.; Singh, A. The Feasibility of Using a Low-Cost near-Infrared, Sensitive, Consumer-Grade Digital Camera Mounted on a Commercial UAV to Assess Bambara Groundnut Yield. *Int. J. Remote Sens.* **2022**, *43*, 393–423. [CrossRef]
31. Du, M.; Noguchi, N. Monitoring of Wheat Growth Status and Mapping of Wheat Yield's within-Field Spatial Variations Using Color Images Acquired from UAV-Camera System. *Remote Sens.* **2017**, *9*, 289. [CrossRef]
32. Zhou, X.; Zheng, H.B.; Xu, X.Q.; He, J.Y.; Ge, X.K.; Yao, X.; Cheng, T.; Zhu, Y.; Cao, W.X.; Tian, Y.C. Predicting Grain Yield in Rice Using Multi-Temporal Vegetation Indices from UAV-Based Multispectral and Digital Imagery. *ISPRS J. Photogramm. Remote Sens.* **2017**, *130*, 246–255. [CrossRef]
33. Wang, L.; Tian, Y.; Yao, X.; Zhu, Y.; Cao, W. Predicting Grain Yield and Protein Content in Wheat by Fusing Multi-Sensor and Multi-Temporal Remote-Sensing Images. *Field Crops Res.* **2014**, *164*, 178–188. [CrossRef]
34. Sun, L.; Gao, F.; Anderson, M.C.; Kustas, W.P.; Alsina, M.M.; Sanchez, L.; Sams, B.; McKee, L.; Dulaney, W.; White, W.A.; et al. Daily Mapping of 30 m LAI and NDVI for Grape Yield Prediction in California Vineyards. *Remote Sens.* **2017**, *9*, 317. [CrossRef]
35. Ranjan, R.; Chandel, A.K.; Khot, L.R.; Bahlol, H.Y.; Zhou, J.; Boydston, R.A.; Miklas, P.N. Irrigated Pinto Bean Crop Stress and Yield Assessment Using Ground Based Low Altitude Remote Sensing Technology. *Inf. Process. Agric.* **2019**, *6*, 502–514. [CrossRef]
36. Pereira, V.G.C.; Gris, D.J.; Marangoni, T.; Frigo, J.P.; De Azevedo, K.D.; Grzesiuck, A.E. Exigências Agroclimáticas Para a Cultura Do Feijão (*Phaseolus Vulgaris* L.) Vinicius. *Rev. Bras. Energ. Renov.* **2014**, *3*, 32–42.
37. Kano, C.; Cardoso, A.I.I.; Villas Bôas, R.L. Influencia de Doses de Potássio Nos Teores de Macronutrientes Em Plantas e Sementes de Alface. *Hortic. Bras.* **2010**, *28*, 287–291. [CrossRef]
38. Canizella, B.T.; Moreira, A.; Moraes, L.A.C.; Fageria, N.K. Efficiency of Magnesium Use by Common Bean Varieties Regarding Yield, Physiological Components, and Nutritional Status of Plants. *Commun. Soil. Sci. Plant Anal.* **2015**, *46*, 1376–1390. [CrossRef]
39. Zhou, J.; Khot, L.R.; Boydston, R.A.; Miklas, P.N.; Porter, L. Low Altitude Remote Sensing Technologies for Crop Stress Monitoring: A Case Study on Spatial and Temporal Monitoring of Irrigated Pinto Bean. *Precis. Agric.* **2018**, *19*, 555–569. [CrossRef]
40. Parker, T.A.; Palkovic, A.; Gepts, P. Determining the Genetic Control of Common Bean Early-Growth Rate Using Unmanned Aerial Vehicles. *Remote Sens.* **2020**, *12*, 1748. [CrossRef]
41. Lipovac, A.; Bezdan, A.; Moravčević, D.; Djurović, N.; Ćosić, M.; Benka, P.; Stričević, R. Correlation between Ground Measurements and UAV Sensed Vegetation Indices for Yield Prediction of Common Bean Grown under Different Irrigation Treatments and Sowing Periods. *Water* **2022**, *14*, 3786. [CrossRef]
42. Santos, H.G.; Jacomine, P.K.T.; Anjos, L.H.C.; Oliveira, V.A.; Lumbreras Coelho, M.R.; Almeida, J.A.; Filho, A.J.C.; de Oliveira, J.B.; Cunha, T.J.F. *Brazilian Soil Classification System*, 5th ed.; Embrapa Soils: Brasília, Brazil, 2018; ISBN 9788570358219.

43. Darim, E.P. Variabilidade Espacial De Atributos Físico-Hídricos Do Solo Em Área Irrigada. Master's Thesis, Programa de Pós-Graduação em Irrigação no Cerrado, Instituto Federal Goiano—Campus Ceres, Ceres, Brazil, 2017; 104p.
44. Peel, M.C.; Finlayson, B.L.; McMahon, T.A. Updated World Map of the Koppen-Geiger Climate Classificatio. *Hydrol. Earth Syst. Sci.* **2007**, *11*, 1633–1644. [CrossRef]
45. Rouse, J.W.; Haas, R.H.; Schell, J.A.; Deering, D.W.; Harlan, J.C. *Monitoring the Vernal Advancements and Retrogradation of Natural Vegetation*; NASA Technical Reports Server (NTRS): Greenbelt, MD, USA, 1974; 137p.
46. Gitelson, A.A.; Merzlyak, M.N. Remote Sensing of Chlorophyll Concentration in Higher Plant Leaves. *Adv. Space Res.* **1998**, *22*, 689–692. [CrossRef]
47. Barnes, E.M.; Clarke, T.R.; Richards, S.E.; Colaizzi, P.D.; Haberland, J.; Kostrzewski, M.; Waller, P.; Choi, C.R.E.; Thompson, T.; Lascano, R.J.; et al. Coincident Detection of Crop Water Stress, Nitrogen Status and Canopy Density Using Ground Based Multispectral Data. In Proceedings of the 5th International Conference on Precision Agriculture, Bloomington, MN, USA, 16–19 July 2000.
48. Daughtry, C.S.T.; Walthall, C.L.; Kim, M.S.; de Colstoun, E.B.; McMurtrey, J.E. Estimating Corn Leaf Chlorophyll Concentration from Leaf and Canopy Reflectance. *Remote Sens. Environ.* **2000**, *74*, 229–239. [CrossRef]
49. Datt, B. A New Reflectance Index for Remote Sensing of Chlorophyll Content in Higher Plants: Tests Using Eucalyptus Leaves. *J. Plant Physiol.* **1999**, *154*, 30–36. [CrossRef]
50. Peñuelas, J.; Frederic, B.; Filella, I. Semi-Empirical Indices to Assess Carotenoids/Chlorophyll a Ratio from Leaf Spectral Reflectance. *Photosynthetica* **1995**, *31*, 221–230.
51. Gitelson, A.A.; Kaufman, Y.J.; Stark, R.; Rundquist, D. Novel Algorithms for Remote Estimation of Vegetation Fraction. *Remote Sens. Environ.* **2002**, *80*, 76–87. [CrossRef]
52. Hunt, R.E.; Daughtry, C.S.T.; Eitel, J.U.H.; Long, D.S. Remote Sensing Leaf Chlorophyll Content Using a Visible Band Index. *Agron. J.* **2011**, *103*, 1090–1099. [CrossRef]
53. Rouse, J.W.; Haas, R.H.; Schell, J.A.; Deering, D.W. Monitoring Vegetation Systems in the Great Plains with ERTS. *NASA Spec. Publ.* **1974**, *351*, 309.
54. Huete, A.R. A Soil-Adjusted Vegetation Index (SAVI). *Remote Sens. Environ.* **1988**, *25*, 295–309. [CrossRef]
55. Huete, A.; Didan, K.; Miura, T.; Rodriguez, E.P.; Gao, X.; Ferreira, L.G. Overview of the Radiometric and Biophysical Performance of the MODIS Vegetation Indices. *Remote Sens. Environ.* **2002**, *83*, 195–213. [CrossRef]
56. Da Silva, J.L.B.; Moura, G.B.d.A.; da Silva, M.V.; de Oliveira-Júnior, J.F.; Jardim, A.M.d.R.F.; Refati, D.C.; Lima, R.d.C.C.; de Carvalho, A.A.; Ferreira, M.B.; de Brito, J.I.B.; et al. Environmental Degradation of Vegetation Cover and Water Bodies in the Semiarid Region of the Brazilian Northeast via Cloud Geoprocessing Techniques Applied to Orbital Data. *J. S. Am. Earth Sci.* **2023**, *121*, 104164. [CrossRef]
57. Gao, B.C. NDWI—A Normalized Difference Water Index for Remote Sensing of Vegetation Liquid Water from Space. *Remote Sens. Environ.* **1996**, *58*, 257–266. [CrossRef]
58. McFEETERS, S.K. The Use of the Normalized Difference Water Index (NDWI) in the Delineation of Open Water Features. *Int. J. Remote Sens.* **1996**, *17*, 1425–1432. [CrossRef]
59. ESA. *Sentinel-2 User Handbook*, 1st ed.; European Space Agency: Paris, France, 2013.
60. Gorelick, N.; Hancher, M.; Dixon, M.; Ilyushchenko, S.; Thau, D.; Moore, R. Google Earth Engine: Planetary-Scale Geospatial Analysis for Everyone. *Remote Sens. Environ.* **2017**, *202*, 18–27. [CrossRef]
61. Tomasella, J.; Silva Pinto Vieira, R.M.; Barbosa, A.A.; Rodriguez, D.A.; de Oliveira Santana, M.; Sestini, M.F. Desertification Trends in the Northeast of Brazil over the Period 2000–2016. *Int. J. Appl. Earth Obs. Geoinf.* **2018**, *73*, 197–206. [CrossRef]
62. Hallak, R.; Pereira Filho, A.J. Metodologia Para Análise de Desempenho de Simulações de Sistemas Convectivos Na Região Metropolitana de São Paulo Com o Modelo ARPS: Sensibilidade a Variações Com Os Esquemas de Advecção e Assimilação de Dados. *Rev. Bras. Meteorol.* **2011**, *26*, 591–608. [CrossRef]
63. Figueiredo, D.B.; Silva Júnior, J.A. Desvendando Os Mistérios Do Coeficiente de Correlação de Pearson (r). *Rev. Política Hoje* **2009**, *18*, 115–146.
64. Mukaka, M.M. Statistics Corner: A Guide to Appropriate Use of Correlation Coefficient in Medical Research. *Malawi Med. J.* **2012**, *24*, 69–71.
65. Jardim, A.M.D.R.F.; Silva, M.V.D.; Silva, A.R.; Santos, A.D.; Pandorfi, H.; Oliveira-Júnior, J.F.D.; de Lima, J.L.M.P.; Souza, L.S.B.D.; Araújo Júnior, G.D.N.; Lopes, P.M.O.; et al. Spatiotemporal Climatic Analysis in Pernambuco State, Northeast Brazil. *J. Atmos. Sol. Terr. Phys.* **2021**, *223*, 105733. [CrossRef]
66. Kaiser, H.F. The Varimax Criterion for Analytic Rotation in Factor Analysis. *Psychometrika* **1958**, *23*, 187–200. [CrossRef]
67. de Oliveira-Júnior, J.F.; de Gois, G.; Silva, I.J.d.L.; de Oliveira Souza, E.; Jardim, A.M.d.R.F.; da Silva, M.V.; Shah, M.; Jamjareegulgarn, P. Wet and Dry Periods in the State of Alagoas (Northeast Brazil) via Standardized Precipitation Index. *J. Atmos. Sol. Terr. Phys.* **2021**, *224*, 105746. [CrossRef]
68. Sokal, R.R.; Rohlf, F.J. The comparison of dendrograms by objective methods. *Taxon* **1962**, *11*, 33–40. [CrossRef]
69. R Core Team. R: A Language and Environment for Statistical Computing. Available online: https://www.r-project.org/ (accessed on 6 February 2023).
70. Yuan, M.; Burjel, J.C.; Martin, N.F.; Isermann, J.; Goeser, N.; Pittelkow, C.M. Advancing On-Farm Research with UAVs: Cover Crop Effects on Crop Growth and Yield. *Agron. J.* **2021**, *113*, 1071–1083. [CrossRef]

71. Tisot, D.A. Modelos de Transferência Radiotiva No Estudo da Concentração de Clorofila em Cana-de-Açúcar, Utilizando Dados Hiperespectrais. 2009. Available online: http://mtc-m16c.sid.inpe.br/col/sid.inpe.br/mtc-m18@80/2009/07.06.19.44/doc/publicacao.pdf (accessed on 30 October 2023).
72. Javed, A.; Ahmad, N.; Ahmed, J.; Hameed, A.; Ashraf, M.A.; Zafar, S.A.; Maqbool, A.; Al-Amrah, H.; Alatawi, H.A.; Al-Harbi, M.S.; et al. Grain Yield, Chlorophyll and Protein Contents of Elite Wheat Genotypes under Drought Stress. *J. King Saud. Univ. Sci.* **2022**, *34*, 102279. [CrossRef]
73. Revill, A.; Florence, A.; MacArthur, A.; Hoad, S.; Rees, R.; Williams, M. Quantifying Uncertainty and Bridging the Scaling Gap in the Retrieval of Leaf Area Index by Coupling Sentinel-2 and UAV Observations. *Remote Sens.* **2020**, *12*, 1843. [CrossRef]
74. Gitelson, A.A.; Kaufman, Y.J.; Merzlyak, M.N. Use of a Green Channel in Remote Sensing of Global Vegetation from EOS- MODIS. *Remote Sens. Environ.* **1996**, *58*, 289–298. [CrossRef]
75. Shaul, O. Magnesium Transport and Function in Plants: The Tip of the Iceberg. *BioMetals* **2002**, *15*, 309–323. [CrossRef] [PubMed]
76. Schmitz, P.K.; Kandel, H.J. Using Canopy Measurements to Predict Soybean Seed Yield. *Remote Sens.* **2021**, *13*, 3260. [CrossRef]
77. Ji, Y.; Chen, Z.; Cheng, Q.; Liu, R.; Li, M.; Yan, X.; Li, G.; Wang, D.; Fu, L.; Ma, Y.; et al. Estimation of Plant Height and Yield Based on UAV Imagery in Faba Bean (*Vicia faba* L.). *Plant Methods* **2022**, *18*, 26. [CrossRef]
78. Spies, G.; Botelho, F.M.; Campos, S.C.; Poltronieri, K.C.; Ruffato, S. Efeito Do Espaçamento de Plantio e o Teor de Água Na Massa Específica e Massa de Mil Grãos Dos Grãos de Soja. In Proceedings of the Quinto Congresso de la Soja del Mercosur, Resumos Rosario, Argentina, 2011; pp. 1–5.
79. Prudente, V.H.R.; Mercante, E.; Johann, J.A.; de Souza, C.H.W.; Cattani, C.E.V.; Mendes, I.S.; Caon, I.L. Use of Terrestrial Remote Sensing to Estimate Soybeans and Beans Biophysical Parameters. *Geocarto Int.* **2021**, *36*, 773–790. [CrossRef]
80. Hussain, S.; Gao, K.; Din, M.; Gao, Y.; Shi, Z.; Wang, S. Assessment of UAV-Onboard Multispectral Sensor for Non-Destructive Site-Specific Rapeseed Crop Phenotype Variable at Different Phenological Stages and Resolutions. *Remote Sens.* **2020**, *12*, 397. [CrossRef]
81. Din, M.; Zheng, W.; Rashid, M.; Wang, S.; Shi, Z. Evaluating Hyperspectral Vegetation Indices for Leaf Area Index Estimation of Oryza Sativa L. at Diverse Phenological Stages. *Front. Plant Sci.* **2017**, *8*, 820. [CrossRef] [PubMed]
82. Zhao, Y.; Potgieter, A.B.; Zhang, M.; Wu, B.; Hammer, G.L. Predicting Wheat Yield at the Field Scale by Combining High-Resolution Sentinel-2 Satellite Imagery and Crop Modelling. *Remote Sens.* **2020**, *12*, 1024. [CrossRef]
83. Bolton, D.K.; Friedl, M.A. Forecasting Crop Yield Using Remotely Sensed Vegetation Indices and Crop Phenology Metrics. *Agric. For. Meteorol.* **2013**, *173*, 74–84. [CrossRef]
84. Moussa Kourouma, J.; Eze, E.; Negash, E.; Phiri, D.; Vinya, R.; Girma, A.; Zenebe, A. Assessing the Spatio-Temporal Variability of NDVI and VCI as Indices of Crops Productivity in Ethiopia: A Remote Sensing Approach. *Geomat. Nat. Hazards Risk* **2021**, *12*, 2880–2903. [CrossRef]
85. da Silva, J.L.B.; Bezerra, A.C.; Moura, G.B.d.A.; Jardim, A.M.d.R.F.; Batista, P.H.D.; de Jesus, F.L.F.; Sanches, A.C.; da Silva, M.V. Spatiotemporal Dynamics of Agricultural Areas with Central Pivot Using Orbital Remote Sensing in the Brazilian Semiarid. *Smart Agric. Technol.* **2022**, *2*, 100052. [CrossRef]
86. Filla, V.A.; Coelho, A.P.; Bettiol, J.V.T.; Leal, F.T.; Lemos, L.B.; Rosalen, D.L. Model Performance in Estimating the Yield of Common Bean Cultivars. *Revista Ciência Agronômica* **2023**, *54*, e20217835. [CrossRef]
87. Barboza, T.O.C.; Ardigueri, M.; Souza, G.F.C.; Ferraz, M.A.J.; Gaudencio, J.R.F.; dos Santos, A.F. Performance of Vegetation Indices to Estimate Green Biomass Accumulation in Common Bean. *AgriEngineering* **2023**, *5*, 840–854. [CrossRef]
88. Ibrahim, E.S.; Rufin, P.; Nill, L.; Kamali, B.; Nendel, C.; Hostert, P. Mapping Crop Types and Cropping Systems in Nigeria with Sentinel-2 Imagery. *Remote Sens.* **2021**, *13*, 3523. [CrossRef]
89. San Bautista, A.; Fita, D.; Franch, B.; Castiñeira-Ibáñez, S.; Arizo, P.; Sánchez-Torres, M.J.; Becker-Reshef, I.; Uris, A.; Rubio, C. Crop Monitoring Strategy Based on Remote Sensing Data (Sentinel-2 and Planet), Study Case in a Rice Field after Applying Glycinebetaine. *Agronomy* **2022**, *12*, 708. [CrossRef]
90. Schwarz, M.; Ouédraogo, W.A.; Traoré, I.; Müller, C.; Sié, A.; Barteit, S.; Mank, I.; Siegert, F.; Sauerborn, R.; Franke, J. Satellite-Based Multi-Annual Yield Models for Major Food Crops at the Household Field Level for Nutrition and Health Research: A Case Study from the Nouna HDSS, Burkina Faso. *Int. J. Appl. Earth Obs. Geoinf.* **2023**, *117*, 103203. [CrossRef]
91. Refati, D.C.; da Silva, J.L.B.; Macedo, R.S.; Lima, R.d.C.C.; da Silva, M.V.; Pandorfi, H.; Silva, P.C.; de Oliveira-Júnior, J.F. Influence of Drought and Anthropogenic Pressures on Land Use and Land Cover Change in the Brazilian Semiarid Region. *J. South. Am. Earth Sci.* **2023**, *126*, 104362. [CrossRef]
92. García-Berná, J.A.; Ouhbi, S.; Benmouna, B.; García-Mateos, G.; Fernández-Alemán, J.L.; Molina-Martínez, J.M. Systematic Mapping Study on Remote Sensing in Agriculture. *Applied Sciences* **2020**, *10*, 3456. [CrossRef]
93. Zhao, L.; Shi, Y.; Liu, B.; Hovis, C.; Duan, Y.; Shi, Z. Finer Classification of Crops by Fusing UAV Images and Sentinel-2A Data. *Remote Sens.* **2019**, *11*, 3012. [CrossRef]

Disclaimer/Publisher's Note: The statements, opinions and data contained in all publications are solely those of the individual author(s) and contributor(s) and not of MDPI and/or the editor(s). MDPI and/or the editor(s) disclaim responsibility for any injury to people or property resulting from any ideas, methods, instructions or products referred to in the content.